Document Number**:** H2020-ICT-52/RISE-6G/D2.4

Project Name:
Reconfigurable **I**ntelligent **S**ustainable **E**nvironments for **6G** Wireless Networks (RISE-6G)

Deliverable D2.4

Metrics and KPIs for RISE wireless systems analysis: final results

Date of delivery:	04/02/2022	Version:	FINAL
Start date of Project:	01/01/2021	Duration:	36 months

Deliverable D2.4

Metrics and KPIs for RISE wireless systems analysis: first results

Project Number:	101017011
Project Name:	**R**econfigurable **I**ntelligent **S**ustainable **E**nvironments for **6G** Wireless Networks

Document Number:	H2020-ICT-52/RISE-6G/D2.4
Document Title:	Metrics and KPIs for RISE wireless systems analysis: first results
Editor(s):	V. Sciancalepore (NEC)
Authors:	M. Crozzoli (TIM), P. Gianola (TIM), T. Svensson (CHAL), A. Clemente (CEA), B. Denis (CEA), M.-H. Hamon (ORA), P. Ratajczak (ORA), Y. Benedic (ORA), S. Herraiz Gonzales (ORA), D.-T. Phan Huy (ORA), G. C. Alexandropoulos (NKUA), K. Katsanos (NKUA), K. Stylianopoulos (NKUA), I. Vinieratou (NKUA), M. Di Renzo (CNRS)
Dissemination Level:	PU
Contractual Date of Delivery:	31/12/2021
Security:	Public
Status:	FINAL
Version:	11
File Name:	RISE-6G_WP2_D2.4_FINAL.docx

Abstract

The current document summarises the final results of the activity devoted to identifying traditional and beyond-SoTA relevant performance metrics and KPIs, to be further used by the technical WPs to assess the performance of RISE wireless systems for different identified scenarios.

A generic downlink system model has been described as the basis to provide the definitions for various performance metrics.

In addition, the concept of “Area of Influence” as the area of significant improvement of wireless connectivity enabled by the RIS technology has been introduced and some corresponding analysis has been performed.

In the end the concept of “Band of Influence” as the frequency bandwidth in which any wave hitting the RIS gets reflected is introduced and some conclusions are derived with reference to the introduction of RIS devices on spectrum coexistence between operators.

Keywords

Beyond-5G; 6G; RIS; KPI; Use cases, Metrics, Localization, Connectivity

Acronyms

Acronym	Definition
2D	Two dimensional
AO	Alternating optimisation
AroI	Area of influence
B5G	Beyond-5G
BS	Base station
CDF	Cumulative distribution function
CEP	Circular error probability
CPU	Central processing unit
DL	Downlink
E2E	End-to-end delay
EE	Energy efficiency
EE-AroI	Energy efficiency boosted – area of Influence
EMF	Electromagnetic field
EMFE	Electromagnetic field exposure
EMFEU	Electromagnetic field exposure utility
EMFEU-AroI	Electromagnetic field exposure utility boosted – area of influence
ES	Edge server
HTR	Hit target radius
I-EMFEU	Inter EMFEU
KPI	Key performance indicator
LB-AroI	Localization boosted – area of influence
LE-AroI	Localization enabled – area of influence
LoS	Line-of-sight
MEC	Multiple-access edge computing
MO	Manifold optimization
MRT	Maximum ratio transmission
MSE	Mean square error
MTBF	Mean-time between failures
NloS	Non-line-of-sight
NMSE	Normalised mean squared error
PEB	Position error bound
PGA	Projected gradient ascent
PIN	Positive-intrinsic-negative
RIS	Reconfigurable intelligent surface
RISE	RIS-Empowered
RMSE	Root mean squared error
RX	Receiver
SE	Spectral efficiency
S-EMFEU	Self electromagnetic field exposure utility
SE-AroI	Spectral efficiency-boosted area of Influence
SINR	Signal-to-noise-plus-interference ratio

SISO	Single input single output
SNR	Signal-to-noise ratio
SoTA	State-of-The-Art
SSE	Secrecy spectral efficiency
UE	User equipment
UL	Uplink

Contents

List of Figures

List of Tables

1 Introduction

The general objective of WP2 is to investigate high relevance Beyond-5G (B5G) scenarios and relevant use cases where the RIS technology can be successfully exploited.

The current document summarises stable results of the activity devoted to identifying the traditional, as well as defining beyond-SoTA, relevant performance metrics and expected key performance indicators (KPIs)[1], to be used by the technical WPs to assess the performance of RIS-Empowered (RISE) wireless systems for different scenarios.

The document is organized into three main sections:

- In section 2, a generic downlink (DL) system model is defined together with the following metrics and KPIs: signal-to-noise ratio (SNR) and signal-to-noise-plus-interference ratio (SNIR), latency, communication reliability, channel estimation accuracy, localization accuracy and integrity, energy efficiency, electromagnetic field exposure utility, and secrecy spectral efficiency.
- In section 3, the concept of “Area of Influence” as the area of significant improvement of wireless connectivity enabled by the RIS technology is introduced, and some analysis is performed on it by starting from the performance analysis of a RISE system optimized for a nominal intended RX position (the “Spatial Focusing” concept).
- In section 4, the concept of “Band of Influence” as the frequency bandwidth in which any wave hitting the RIS gets reflected is introduced and, after an experimental investigation of the behaviour of a RIS, some conclusions are derived with reference to the introduction of a RIS on spectrum coexistence between operators.

[1] Note that target KPIs will be further discussed along with RISE-6G field-trials setup and evaluation details within Deliverable D7.1.

2 Metrics and key performance indicators

In this section, we provide first examples of key definitions and KPIs, which are used to evaluate the performance benefits brought by RISs.

In the current deliverable, we consider the DL direction only, unless it is strictly necessary to consider UL as well (for example, in the calculation of the two-way latency). However, for most metrics, the uplink (UL) definition can be derived in a similar manner by taking into account that the most important differences in UL as compared to DL are: (1) the need to coordinate the transmitters in the uplink through random access algorithms, scheduling or a combination thereof and (2) the power constraints are per terminal, while in the DL there is a single power constraint for the BS.

This section is organised as follows: sub-section 2.1 describes the generic DL system model that will be referred to in most consecutive sub-sections; sub-sections 2.2 to 2.11 provide the proposed definitions for various performance metrics.

2.1 Downlink generic system model, signal to noise ratio and signal to noise and interference ratio

We consider a base station (BS) equipped with M antennas, K single-antenna intended user equipment (UE) and a RIS, which is modeled as a planar array with $N = N_x \times N_y$ radiating elements, where N_x and N_y are the number of radiating elements along the x and y axis, respectively.

In this deliverable, we model the BS-to-RIS propagation channel as a Ricean-faded channel such that

$$\mathbf{G}_k = \sqrt{\gamma_G}\sqrt{\frac{\kappa_G}{1+\kappa_G}}\,\mathbf{a}(\boldsymbol{\theta}_A)\mathbf{b}(\boldsymbol{\theta}_D)^{\mathrm{H}} + \sqrt{\frac{1}{1+\kappa_G}}\mathbf{H}^{NLoS} \in \mathbb{C}^{N\times M},$$

where γ_G is the average pathloss gain, κ_G is the Rician factor (for $\kappa_G = 0$, the Rayleigh fading case appears, whereas a pure line-of-sight channel happens when κ_G takes large positive values), $[.]^{\mathrm{H}}$ is the Hermitian operation, and $\mathbf{H}^{NLoS} \in \mathbb{C}^{N\times M}$ represents the random non-line-of-sight (NLoS) part comprising zero-mean and unit-variance elements. In the latter expression, the antenna array responses at the BS and at the RIS, respectively, for the steering angles θ_A (angle-of-arrival) and θ_D (angle-of-departure), respectively, are defined as:

$$\mathbf{a}(\boldsymbol{\theta}_A) = \left[1, e^{j2\pi\frac{d}{\lambda}\cos(\theta_A)}, \ldots, e^{j2\pi\frac{d}{\lambda}(N-1)\cos(\theta_A)}\right]^T \in \mathbb{C}^{N\times 1}$$

and

$$\mathbf{b}(\boldsymbol{\theta}_D) = \left[1, e^{j2\pi\frac{d}{\lambda}\cos(\theta_D)}, \ldots, e^{j2\pi\frac{d}{\lambda}(M-1)\cos(\theta_D)}\right]^T \in \mathbb{C}^{M\times 1}$$

with $\frac{d}{\lambda}$ being the ratio between the antenna element spacing and the signal wavelength with $d = \lambda/2$.

The wireless channel between the RIS and each k-th UE is also modeled as Ricean:

$$\mathbf{h}_k = \sqrt{\gamma_k}\sqrt{\frac{\kappa_k}{1+\kappa_k}}\,\mathbf{b}(\boldsymbol{\theta}_k) + \sqrt{\frac{1}{1+\kappa_k}}\mathbf{h}_k^{NLoS} \in \mathbb{C}^{N\times 1},$$

where γ_k is the average pathloss gain, κ_k is the Rician factor, and $\mathbf{h}_k^{NLoS} \sim \mathcal{CN}(0, \mathbf{\Sigma})$ represents the random non-line-of-sight (NLoS) part. Finally, we represent the direct link between the BS and UE k as $\mathbf{h}_{d,k} \in \mathbb{C}^{M\times 1}$, which is also modeled as Ricean faded.

Let $\mathbf{\Phi} = \text{diag}(\phi_1, \dots, \phi_N) \in \mathbb{C}^{N\times N}$ be the matrix containing the applied phase shifts $\{\phi_n\}_{n=1}^N$ with $|\phi_n|^2 \leq 1, \ \forall\, n$ from the RIS. Furthermore, we define the multi-user precoding matrix at the BS as $\mathbf{W} = [\mathbf{w}_1, \dots, \mathbf{w}_K] \in \mathbb{C}^{M\times K}$ with $\|\mathbf{W}\|_F^2 \leq P$ (P is the total BS transmit power) and the data symbol vector $\boldsymbol{s} = [s_1, \dots, s_K]^T \in \mathbb{C}^{K\times 1}$ where each s_k is intended for UE k with $\mathbb{E}[|s_k|^2] = 1, \ \forall\, k$. Lastly, we let n_k denote the additive white Gaussian noise coefficient distributed as $\mathcal{CN}(0, \sigma^2)$. The received signal at a given UE k is expressed as

$$\boldsymbol{y_k} = \left(\mathbf{h}_k^{\boldsymbol{H}}\mathbf{\Phi}\mathbf{G} + \mathbf{h}_{d,k}^{\mathbf{H}}\right)\mathbf{W}\mathbf{s} + \boldsymbol{n_k} \in \mathbb{C}.$$

Hence, the signal-to-noise ratio (SNR) of UE k is defined as

$$\mathbf{SNR}_{\boldsymbol{k}} = \frac{\left|\left(\mathbf{h}_{\boldsymbol{k}}^{\mathbf{H}}\mathbf{\Phi}\mathbf{G} + \mathbf{h}_{\boldsymbol{d,k}}^{\mathbf{H}}\right)\mathbf{w}_{\boldsymbol{k}}\right|^{\mathbf{2}}}{\boldsymbol{\sigma^2}},$$

and, consecutively, the signal-to-interference-plus-noise ratio (SINR) of UE k is given by

$$\mathbf{SINR}_{\boldsymbol{k}} = \frac{\left|\left(\mathbf{h}_{\boldsymbol{k}}^{\boldsymbol{H}}\mathbf{\Phi}\mathbf{G} + \mathbf{h}_{\boldsymbol{d,k}}^{\mathbf{H}}\right)\mathbf{w}_{\boldsymbol{k}}\right|^{\mathbf{2}}}{\sum_{\boldsymbol{j}\neq\boldsymbol{k}}\left|\left(\mathbf{h}_{\boldsymbol{k}}^{\boldsymbol{H}}\mathbf{\Phi}\mathbf{G} + \mathbf{h}_{\boldsymbol{d,k}}^{\mathbf{H}}\right)\mathbf{w}_{\boldsymbol{j}}\right|^{\mathbf{2}} + \boldsymbol{\sigma^2}}. \quad (1)$$

In the next steps of the research activity this definition will be extended to any type of propagation channel.

2.2 Spectral efficiency and throughput

In this sub-section, we provide an example of definition of the **spectral efficiency (SE)** metric, which concerns the rate of reliably transmitted information over the allocated communication bandwidth B. Formally, the achievable SE with respect to a UE depends on the UE's SINR. For instance, with the notation defined in (1), the achievable SE of a UE *k* is given by

$$\mathbf{SE}_{\boldsymbol{k}} = \mathbf{log_2}(\mathbf{1} + \mathbf{SINR}_{\boldsymbol{k}}) \quad \mathbf{(bits/s/Hz)}, \quad (2)$$

and accordingly, the *individual-rate over its allocated bandwidth* is defined as

$$\boldsymbol{\mathcal{R}_k} = \mathbf{SE}_{\boldsymbol{k}}\, \boldsymbol{B_k}.$$

The throughput of the considered system is finally given by:

$$\boldsymbol{T} = \sum_{\boldsymbol{k}} \boldsymbol{\mathcal{R}_k}.$$

2.3 Latency

Latency is one of the key performance metrics defined in 5G and B5G multiple-access edge computing (MEC) systems. Several applications (e.g., autonomous driving, industry 4.0, etc.) pose a very strict requirement on the end-to-end (E2E) latency, which in many cases must be in the order of 1ms or even less. The definition of E2E latency in the MEC context depends on the kind of computation offloading request, which can be categorised as either static or dynamic.

2.3.1 Static computation offloading

Static computation offloading deals with short time applications, in which mobile UEs send a single computation request, typically also specifying a service time. Let $A_k(t)$ be the number of input bits required by the application run by user k at time t, and let $w_k(t)$ be the number of central processing unit (CPU) cycles associated with the computing task. Then, the overall E2E

delay of UE k is composed of three terms: (i) an UL communication time $\Delta_k^u(t)$, needed by the device to send the input bits to the BS; (ii) a computation time $\Delta_k^c(t)$, needed by the edge server (ES) to process the input bits and run the specific application; (iii) a DL communication time $\Delta_k^d(t)$, needed by the BS to send the result of computation back to the UE(s).

In summary, the overall E2E latency at time t is given by:

$$\Delta_k(t) = \Delta_k^u(t) + \Delta_k^c(t) + \Delta_k^d(t) = \frac{A_k(t)}{R_k(t)} + \frac{w_k(t)}{f_k(t)} + \frac{B_k(t)}{R_k^d(t)}, \quad (3)$$

where $R_k(t)$ is the uplink rate from UE k to the BS, $f_k(t)$ is the CPU frequency allocated by the edge server to UE k, $R_k^d(t)$ is the downlink rate from the BS to UE k, and $B_k(t)$ is the number of output bits of the application run by the ES on behalf of UE k. In static computation offloading, communication and computation resources are orchestrated to guarantee that the overall E2E delay $\Delta_k(t)$ is less than or equal to an application-dependent requirement, say L_k for all t.

2.3.2 Dynamic computation offloading

In *dynamic computation offloading*, each device continuously generates data $A_k(t)$ to be processed, sometimes with an unknown rate (e.g., the transmission of a video recorded by a mobile device to be processed by the edge server (ES) for pattern recognition or anomaly detection). Then, a queueing system is used to model and control the dynamic data generation, transmission, and processing. At each time slot t, each user buffers data in a local queue $Q_k^l(t)$ and transmits them to the AP at the transmission rate $R_k(t)$. The local queue update follows the rule:

$$Q_k^l(t+1) = max\left(0, Q_k^l(t) - \tau R_k(t)\right) + A_k(t)$$

where τ is the duration of the time-slot used for scheduling the resources.

Then, the BS receives data from each device k and send the data to the ES, which processes J_k bits-for-cycle, where J_k is a parameter that depends on the application offloaded by device k. Thus, the computation queue at the ES evolves as:

$$Q_k^c(t+1) = \max(0, Q_k^c(t) - \tau f_k(t) J_k) + \min(Q_k^l(t), \tau R_k(t))$$

Finally, the BS sends back to each user the bits resulting from the computation, draining a downlink communication queue that evolves as:

$$Q_k^d(t+1) = \max\left(0, Q_k^d(t) - \tau R_k^d(t)\right) + c_k \min(Q_k^c(t), \tau f_k(t) J_k),$$

where c_k denotes the ratio between output and input bits of the application required by user k. Thus, the E2E delay experienced by offloaded data is related to the sum of the three queues:

$$Q_k^{tot}(t) = Q_k^l(t) + Q_k^c(t) + Q_k^d(t).$$

In fact, from the Little's law, given a data arrival rate $\bar{A}_k = \mathbb{E}[A_k(t)]$, (where $\mathbb{E}[.]$ is the expectation) the overall long-term average latency experienced by a new data unit from its generation to its computation at the ES is:

$$\bar{D}_k = \lim_{T\to\infty} \frac{1}{T} \sum_{t=1}^{T} \mathbb{E}\left[\frac{Q_k^{tot}(t)}{\bar{A}_k}\right]$$

where the expectation is taken with respect to the radio channel and data arrival statistics.

Thus, in this dynamic context, an average E2E delay constraint can be written as:

$$\lim_{T\to\infty} \frac{1}{T} \sum_{t=1}^{T} \mathbb{E}[Q_k^{tot}(t)] \leq Q_k^{avg} = D_k^{avg} \bar{A}_k . \quad (4)$$

More sophisticated probabilistic constraints can also be imposed on the maximum tolerable delay.

2.3.3 Expected impact of RIS

Of course, the presence of RISs will impact both UL and DL communication delays, enabling MEC with low latency guarantees also in the presence of poor wireless channel conditions due to, e.g., blocking events, and mobility of the UE(s) and the environment.

2.4 Communication reliability

Given the definitions provided in section 2.1, we define the notion of ***reliability*** of the communication by considering a given minimum SINR threshold denoted as t, which is necessary to decode the incoming signal. Reliability is proportional to the probability that the varying wireless signal is larger than the threshold. We define the set of UE(s) whose received SINR is greater than t as

$$\mathcal{U} = \{k : \mathbf{SINR}_k \geq t\}. \tag{5}$$

RIS-enabled systems are expected to enlarge the network area in which the received SINR of a given UE in said area is above the threshold, and thus, sufficient for successful decoding of the incoming signal.

2.5 Channel estimation accuracy

For the specific problem of channel estimation, we consider the ***normalised mean squared error*** (NMSE) metric to assess the performance of the estimation process. Specifically, NMSE (in dB) can be defined as

$$\mathbf{NMSE} = \mathbb{E}\left[\frac{10\log_{10}\|\mathbf{H}-\hat{\mathbf{H}}\|_F^2}{\|\mathbf{H}\|_F^2}\right], \tag{6}$$

where $\mathbf{H}$ and $\hat{\mathbf{H}}$ denote the true and estimated channel matrices, respectively, and $\|\cdot\|_F$ denotes the Frobenius norm.

2.6 Localisation accuracy

The ***localisation accuracy*** is fundamentally determined by the statistics of the localization error $\mathbf{e} = \mathbf{x} - \hat{\mathbf{x}}$ ($\mathbf{x}$ is the true position and $\hat{\mathbf{x}}$ is the estimated position), comprising horizontal (XY) and vertical (Z) errors.

The statistics include:

- Mean Square Error (MSE): $\mathbb{E}[\mathbf{e}^T\mathbf{e}]$;
- Root MSE (RMSE): $\sqrt{\mathbb{E}[\mathbf{e}^T\mathbf{e}]}$;
- Accuracy (with confidence level α): $Pr(\|\mathbf{e}\| < e) = \alpha$;
- Horizontal accuracy (with confidence level α): $Pr(\|\mathbf{e}_{1:2}\| < e) = \alpha$;
- Vertical accuracy (with confidence level α): $Pr(|e_3| < e) = \alpha$.

The accuracy levels rely on the (empirical) *cumulative distribution function* (CDF) of localisation estimation errors. The CDF is often used to characterise characteristic error values (e.g., so-called “worst case” localization errors at arbitrary high CDF values, typically 90% or 99%). Accordingly, they can reflect more accurately effects such as heavy-tailed/asymmetric localization error distributions, beyond indicators such as MSE.

From these fundamental metrics, additional metrics such as *circular error probability* (CEP) and *hit target radius* (HTR) can be derived. CEP is defined as the probability for a location estimate

to fall into a circle (resp. sphere) of radius R centred around the ground-truth location in 2D (resp. 3D). HTR corresponds to CEP equal to 50%.

The **position error bound** (PEB) indicator is a theoretical performance indicator accounting for the best localisation accuracy achievable by any unbiased estimator, assuming the statistics of available observed/measured radio metrics and, possibly, some a-priori knowledge on UE location. The PEB is defined form the Fisher information matrix **J**, which is a theoretical lower bound on the error covariance, under certain technical condition:

$$\mathbf{J}^{-1}(\mathbf{x}) \preccurlyeq \mathbb{E}[(\mathbf{x}-\hat{\mathbf{x}})(\mathbf{x}-\hat{\mathbf{x}})^{\mathbf{T}}].$$

The PEB (expressed in meters) at a location ***x*** is then defined as

$$\mathbf{PEB}(\mathbf{x}) = \sqrt{\mathbf{trace}\left(\mathbf{J}^{-1}(\mathbf{x})\right)} \leq \sqrt{\mathbb{E}[\|\mathbf{x}-\hat{\mathbf{x}}\|^{2}]}. \quad (7)$$

The PEB can be evaluated as a function of the UE location and represented as a heatmap over a scene.

2.7 Localisation-related delays

As localisation is often time-sensitive and sometimes safety-critical, there are also delay metrics. These include:

- ***First time to fix***: time until the system provides the first location estimate;
- **Localisation *latency***: time between a positioning request and the position being available;
- ***Update rate***: time between successive position estimates.

2.8 Localization integrity

In certain critical applications, the localisation error cannot exceed certain safe thresholds and the localisation service must be available without interruption. Relevant metrics in this regard are:

- ***Reliability***: measured by mean-time between failures (MTBF) or duration of the time in which the service is available;
- ***Availability***: fraction of the time the service is available.

High reliability means high availability, but not the other way around. Hence, a system that is down (i) every other minute for 1 minute or (ii) every other hour for 1 hour has the same availability, but very different reliability.

2.9 Energy efficiency

In this sub-section, we define the ***energy efficiency*** (EE) metric for a DL data communication from a BS to a UE as follows:

$$\boldsymbol{EE = R/P}, \quad (8)$$

where R is the sum data *spectral efficiency* (accounting for *overhead* as in [ZDR+21-1][ZDR+21-2]) in bit/s/Hz and P is the total power consumption in watts for providing the target service, as in [HZA+19].

To allow a fair comparison between state-of-the-art systems and beyond state-of-the-art systems, P must include all significant sources of power consumption. In Table 2-1 au-dessous, we provide a first list of contributions to the total power consumption.

	energy spent by	for what	nature of spent energy
P_1	BS(s)	Sending DL pilots to UE	Radiated power
P_2	UE(s)	Sending UL feedback to base station	
P_3	BS (s)	Sending data	
P_4	BS (s)	All except radiated power	Hardware
P_5	UE(s)	All except radiated power	
P_6	RIS(s)	Reconfiguring and remaining in a given configuration	Hardware
P_7	BS (s) + UE(s)	RIS control channel consumption[2]	Radiated power

Table 2-1 – Sources of power consumption.

With such definition, the power consumptions P^{REF} and P^{RIS} in a network without and with RIS, respectively, are given by the following formulas:

$$P^{REF} = P_1 + P_2 + P_3 + P_4 + P_5$$

and

$$P^{RIS} = P_1 + P_2 + P_3 + P_4 + P_5 + P_6 + P_7$$

Note that the exact expressions of the power consumptions due to radiated power (P_1 to P_3, and P_7), highly differ from one system to another and strongly depend on signalling protocols and overhead. Some detailed examples are available in [ZDR+21-1], [ZDR+21-2] and [HZA+19].

Note that the power consumption due to the RIS hardware (P_6) is expected to increase linearly with the number of unit cells in the RIS.

For instance, in a first example of RIS implementation [FPH+21-1] [FPH+21-2], where each unit cell of the RIS is reflecting incident waves with a phase-shift that is continuously controlled by four varactors (see Figure 2-1 a), the energy consumption of the RIS can be approximated by [RBF+10][RBF+13]:

$$P_6 \sim P_{cc} + P_{cell} \times N$$

where N is the number of unit cells, P_{cc} is the consumption of the RIS control circuit (mainly a micro-controller connected to all unit-cells), P_{cell} is the consumption per unit-cell (accounting for the varactors, digital potentiometers, logical switches, etc.). Note that such model is used in [HZA+19].

In a second example of RIS implementation based on positive-intrinsic-negative (PIN) diodes, where a unit cell is controlled via two diodes (see Figure 2-1 b), and where the diodes are themselves controlled by using a bias current in the range of 1-20 mA and a forward voltage between 1.33V and 1.45V [CDS+12][CDS+13][DPC+17][DCS+20][CDP+20], the same kind of linear dependency of the power with the number of unit cells N applies. In this implementation,

$$P_{cell} \sim Nbl.Vf.Ibias,$$

where, Nbl is the number of bias lines for unit-cells, Vf is the forward voltage and $Ibias$ is the bias current.

[2] This control channel is not just a unidirectional transmission from the BS, but it will involve a full protocol stack for reliable exchange of information; it can be both in-band and out-of-band channel.

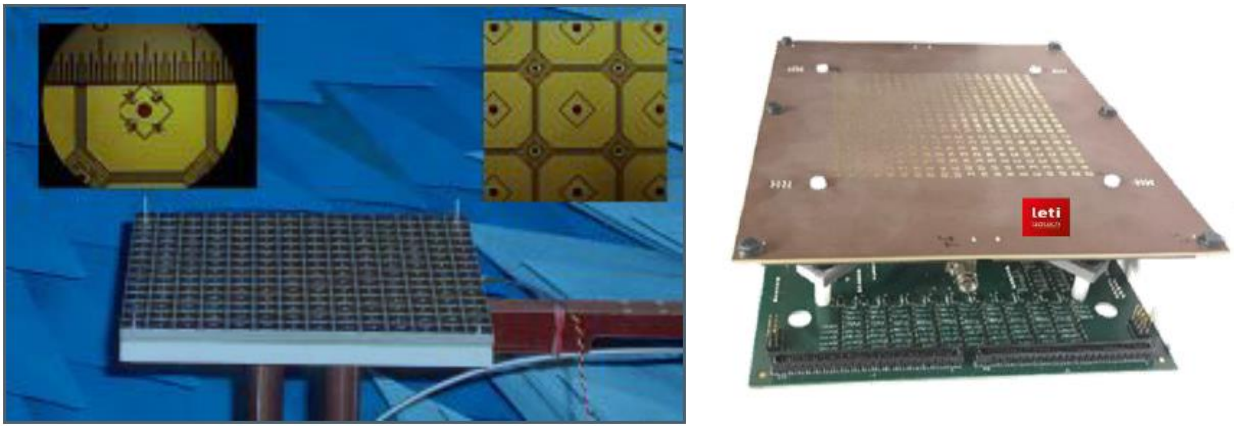

a) Varycap based RIS b) PIN-Diode based RIS

Figure 2-1 – Example of RIS hardware implementations with a) Varycap [RFB+10] and b) PIN diode [CDS+12].

Also, to this stage, it is not yet clear, whether some P_i's can be neglected compared to others. For instance, it has to be checked during the project whether the hardware consumption of RIS(s) can be neglected, or not, compared to the hardware consumption of BS(s) and UE(s) (i.e. it has to be verified whether $P_6 \ll P_5$ and $P_6 \ll P_4$ applies).

2.10 Electromagnetic field exposure utility

In this sub-section, in addition to the DL case, we also consider the UL case.

We first consider as a target service, a DL data communication towards an intended UE. We also consider a non-intended UE who is potentially exposed to the electromagnetic field (EMF) generated by this link. For this target service, we propose the following definition of the ***inter electromagnetic field exposure (EMFE) utility (EMFEU)***:

$$\boldsymbol{EMFEU_{inter} = R^{DL}/X^{NI}}, \quad (9)$$

where R^{DL} is data rate that is delivered to the intended UE and X^{NI} is the EMF to which the non-intended UE is exposed. In the case where we are considering multiple non-intended UEs, X^{NI} is the EMF of the most exposed one.

We then consider as a target service, an UL data communication issued by an intended UE. In this case, the intended UE is also the exposed one. For this target service, we propose the following definition of the **self EMFEU**:

$$\boldsymbol{EMFEU_{self} = R^{UL}/X^{I}}, \quad (10)$$

where R^{UL} is data rate that is transmitted by the intended user and X^{I} is the EMF to which the intended UE is exposed. This refers to the user own radiation, which should be a very local phenomenon. A RIS can help boosting the self EMFEU through improving the link's quality, hence, allowing the UE can achieve the same rate with a lower transmit power and a lower self EMFE.

2.11 Secrecy spectral efficiency

The ***secrecy spectral efficiency*** (SSE) metric is defined as the difference between the intended receiving UE (RX)'s rate R_I, referring to the legitimate link, and the non-intended RX's rate R_{NI}, referring to the link between the legitimate transmitter and the eavesdropper. When

this difference results in a negative number, it means that no security is guaranteed, and the SSE is defined as zero.

Putting all above together, the mathematical definition of SSE is given by

$$\boldsymbol{SSE} = \mathbf{max}(\mathbf{0}, \boldsymbol{R_I} - \boldsymbol{R_{NI}}) \quad (\mathbf{bits/s/Hz}) \tag{11}$$

where $R_I = \log_2(1 + SNR_I)$ and $R_{NI} = \log_2(1 + SNR_{NI})$ with SNR_l being defined as in sub-section 2.1, while SNR_{NI} is defined in a similar way by considering the BS to the non-intended UE direct channel $\mathbf{g}_d$ and the RIS to the non-intended UE channel $\mathbf{g}$.

3 RIS Area of Influence

In this section, we investigate the spatial distribution of the RIS-optimised performance over a geographical area under consideration for the connectivity-related metrics and KPIs of subsections 2.1 to 2.11. To that end, we first study how the performance of a RIS-empowered system optimised for a nominal intended RX position is distributed in space (i.e. the "***Spatial Focusing***") in sub-section 3.1 and its subsections. Building on those results, we define the more general notion of the ***Area of Influence (AroI)***, which concerns the areas of significant improvement of wireless connectivity, when optimising for the entirety of the area under consideration, instead of a single nominal RX position.

It is worth noting that the concept of AroI can refer to the aggregated beneficial effects of multiple RISs that are controlled simultaneously in a given environment (not restricting to single-RIS).

3.1 Investigation of the RIS spatial focusing

Simulations presented in the following sub-sections show that the improvement brought by the RIS optimisation, with respect to each of the considered connectivity metrics, is localised in space. In detail, we devise a common setup comprising a single TX, a single RIS, and a single intended RX, and potentially an attenuator/blocker, and we optimise the system parameters for the position of the nominal intended RX. We visually demonstrate that, for all metrics and considering a Ricean-faded channel with a strong LoS component, the substantial improvement of the performance, in general, lies on the path of the RIS-RX link, as well as the TX-RIS link, in the cases without the attenuator.

3.1.1 Spatial focusing of SE

To investigate the spatial locality of the SE improvement, we first consider a scenario where an *M*-antenna BS transmits data to a single-antenna RX, under either the absence or the presence of a RIS comprising of L unit elements. Specifically, the problem of maximising the achievable rate is formulated first and then solved with optimisation variables the BS precoder $\mathbf{w} \in \mathbb{C}^{M\times 1}$ and the passive beamforming diagonal matrix $\mathbf{\Phi} \in \mathbb{C}^{L\times L}$ for the surface. We denote $\mathbf{h}_d \in \mathbb{C}^{1\times M}$, $\mathbf{h} \in \mathbb{C}^{1\times L}$ and $\mathbf{H}_1 \in \mathbb{C}^{L\times M}$, as the matrices of the direct BS-to- RX, RIS-to-RX and the BS to RIS propagation channel, respectively. To this end, the joint design of these variables is expressed as

$$\boldsymbol{max}_{\mathbf{w},\mathbf{\Phi}} \ \boldsymbol{log}_2\left(\mathbf{1}+\frac{\boldsymbol{P}}{\boldsymbol{\sigma^2}}|(\mathbf{h}_d+\mathbf{h}\mathbf{\Phi}\mathbf{H}_1)\mathbf{w}|^2\right)$$
$$\boldsymbol{s.t.}: \|\mathbf{w}\|^2 \leq \mathbf{1}, \ \left|\mathbf{\Phi}_{l,l}\right| = \mathbf{1} \ \forall \ \boldsymbol{l} = \mathbf{1}, \mathbf{2}, \ldots, \boldsymbol{L}.$$

In the case where the RIS is not present, the above problem reduces to a special version which is solved by setting the precoder $\mathbf{w}$, equal to the maximal ratio transmission (MRT) precoding vector considering the direct channel $\mathbf{h}_d$. Next, to solve the above joint problem, an alternating optimization (AO) approach is adopted, according to which each variable is solved separately until a convergence criterion is met. Then, $\mathbf{w}$ can be solved in closed form, by considering MRT precoding (based on the channel: $\mathbf{h}_d + \mathbf{h}\mathbf{\Phi}\mathbf{H}_1$), and for $\mathbf{\Phi}$ a Riemannian manifold optimization (MO) approach is utilised.

To illustrate the results for both above scenarios, we consider a square grid area with each side being equal to 25m, where the BS is fixed at the point [0 m, 10 m] of the *xy*-plane. Also, the optimisation problem is solved for a certain position of RX, whose coordinates are [15 m, 5 m]. Then, the obtained active and passive beamforming vectors of the nominal position are used to compute the achievable rates for all possible locations inside the grid, to reveal the locality in the considered two-dimensional (2D) area and observe the influence of a RIS when present and located at [10 m, 0 m] The other simulation-setup parameters are presented in the table below and the results are averaged over 100 channel realizations.

Parameter	Value	Parameter	Value
$\boldsymbol{P}$	30 dBm	M	8
$\boldsymbol{\sigma^2}$	-90 dBm	L	100
$\boldsymbol{\kappa}$	13.2 dB	Pathloss Exponent	2.4

Table 3-1 – Simulation parameters.

Next, in Figure 3-1 below the 2D heatmap for the achievable SE in bits/s/Hz and its spatial distribution is illustrated for the cases of the absence and presence of a RIS. Since the LoS component is strong, due to the considered Rician factor κ, some beam patterns appear in the grid area, which are stronger in terms of rate values at the direction that connects the BS with RX's nominal position. On the other hand, when placing a RIS at the location [10, 0], it is depicted in the right subfigure, that almost the whole area gets boosted, in the sense that larger EE values are observed when compared to the case without RIS. Moreover, an enhanced line pattern of rate values is observed as well, at the line that connects the RIS with RX's nominal position. Moreover, it is observed that in contrast to the case of the absence of a RIS, the main beam pattern starting from the BS and heading to nominal RX, is shifted on the right subfigure heading to the RIS which is in turn concentrated to nominal RX's position. This is reasonable, since it shows that the optimization process is in terms of the compound channel $\mathbf{h}_d + \mathbf{h}\boldsymbol{\Phi}\mathbf{H}_1$.

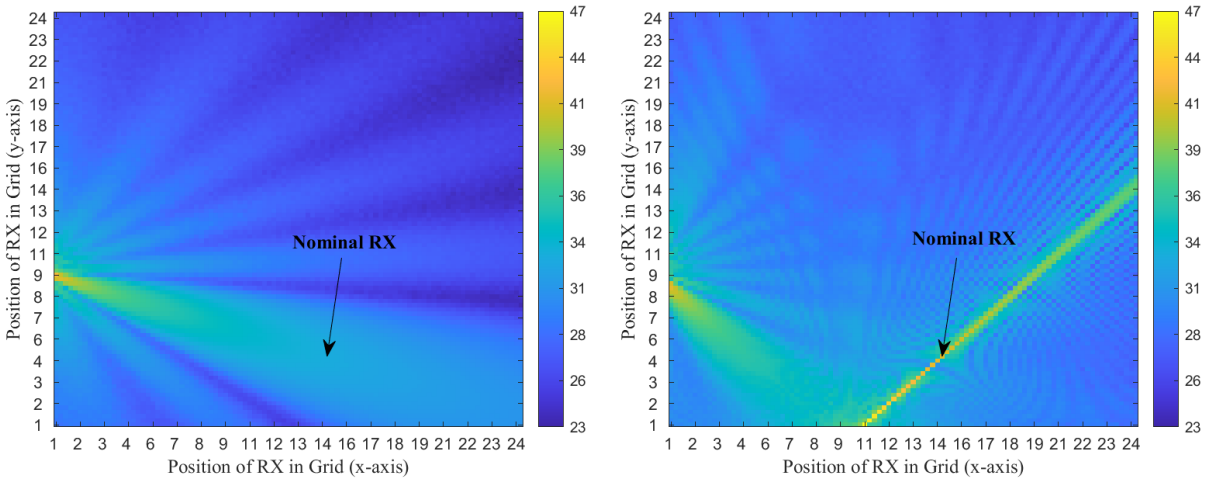

Figure 3-1 – SE values on a 2D grid.
(Left) without the presence of a RIS. (Right) with a RIS placed at [10, 0].

To further show the effects of spatial focusing for SE when a RIS is present, we next introduce an attenuation factor for the LoS component of the direct channel $\mathbf{h}_d$ between the BS and RX, which is considered equal to 0.01 (i.e., 100 dB attenuation). The results for this case are presented in Figure 3-2, where it is evident that in the case of attenuation there is nearly no LoS channel component and the channel's Rayleigh component is thus dominant, such that small SE values are observed. However, when placing a RIS the whole area gets boosted and especially the line that connects the surface with the nominal RX's position.

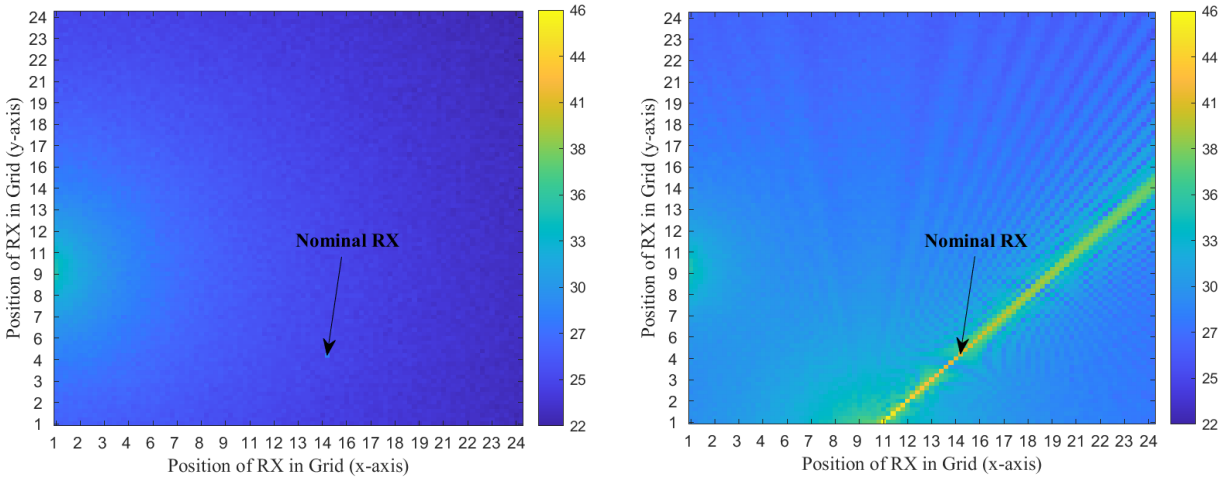

Figure 3-2 – SE values on a 2D grid.
(Left) without the presence of a RIS. (Right) with a RIS placed at [10, 0] with attenuation.

3.1.2 Spatial focusing of SSE

To investigate the spatial locality of the SSE improvement, a scenario with an *M*-antenna BS is considered which attempts to transmit secret single stream data to a single-antenna RX, where a single-antenna eavesdropper is present at the system. To further safeguard the legitimate system [AKW+21], a RIS is also employed under the control of the BS that designs both the precoding vector $\mathbf{w}$ and the passive beamforming diagonal matrix $\mathbf{\Phi}$. Specifically, using the same notations $\mathbf{g}_d$ and $\mathbf{g}$, as in sub-section 2.11, for the BS to the non-intended user direct channel and the RIS to the non-intended user channel, respectively. These design variables are modelled as the solution to the following optimisation problem:

$$\boldsymbol{max}_{\mathbf{w},\mathbf{\Phi}} \ \boldsymbol{log}_2\left(\mathbf{1}+\frac{\boldsymbol{P}}{\boldsymbol{\sigma^2}}|(\mathbf{h}_d+\mathbf{h}\mathbf{\Phi}\mathbf{H_1})\mathbf{w}|^2\right)-\boldsymbol{log}_2\left(\mathbf{1}+\frac{\boldsymbol{P}}{\boldsymbol{\sigma^2}}|(\mathbf{g}_d+\mathbf{g}\mathbf{\Phi}\mathbf{H_1})\mathbf{w}|^2\right)$$
$$\boldsymbol{s.t.}: \|\mathbf{w}\|^2 \leq \mathbf{1}, \ \left|\mathbf{\Phi}_{l,l}\right| = \mathbf{1} \ \forall \ \boldsymbol{l}=\mathbf{1},\mathbf{2},\dots,\boldsymbol{L},$$

where the first term in the objective expresses the legitimate rate and the second one the eavesdropper's rate; their subtraction is the instantaneous SSE performance metric as defined in sub-section 2.11. The solution approach to the above problem is AO, due to the coupled variables and the non-convex objective/constraints. Specifically, to find $\mathbf{w}$ for a fixed $\mathbf{\Phi}$ it suffices to observe that it can be given as the unit-norm eigenvector of the matrix:

$$\left(\mathbf{I}_N+\frac{\boldsymbol{P}}{\boldsymbol{\sigma^2}}\tilde{\mathbf{g}}^H\tilde{\mathbf{g}}\right)^{-1}\left(\mathbf{I}_N+\frac{\boldsymbol{P}}{\boldsymbol{\sigma^2}}\tilde{\mathbf{h}}^H\tilde{\mathbf{h}}\right),$$

which corresponds to its largest eigenvector, and $\tilde{\mathbf{g}}=\ \mathbf{g}_d+\mathbf{g}\mathbf{\Phi}\mathbf{H}_1, \tilde{\mathbf{h}}=\ \mathbf{h}_d+\mathbf{h}\mathbf{\Phi}\mathbf{H}_1$. Next, for a fixed $\mathbf{w}$, $\mathbf{\Phi}$ can be found based on a Riemannian MO or projected gradient ascent (PGA) approach.

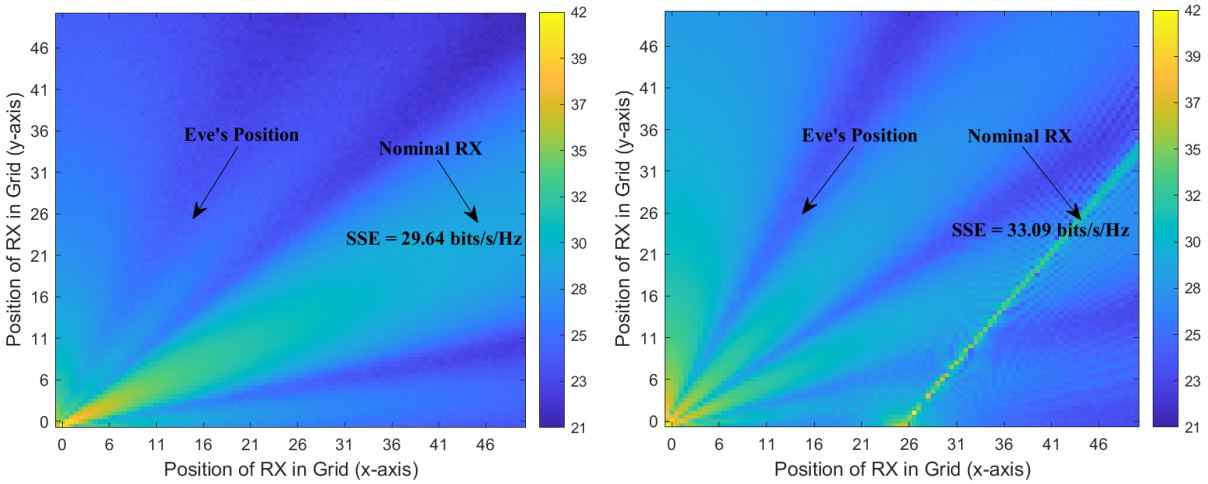

Figure 3-3 – SSE values on a 2D grid within the presence of an eavesdropper (Eve). (Left) without the presence of a RIS. (Right) with a RIS placed at [0, 25].

In Figure 3-3, the results for the SSE are depicted in the case of the absence (on the left) and the presence (on the right) of a RIS with 100 unit elements. The simulation parameters are set similar to those given in Table 3-1. The eavesdropper's position is at the point [10.5 m, 20.5 m] from the BS which is placed at the origin. Also, the nominal position of RX is at [40.5 m, 20.5 m]. When a non-intended user is present even closer to the BS than RX, it is observed that the presence of a RIS boosts the whole area with higher SSE values. Interestingly, a strong beam pattern is observed in the direction which connects the RIS with RX.

3.1.2.1 Spatial focusing of communication reliability

Given the definitions provided in sub-section 3.1.1 and sub-section 2.1, the received signal at a given position k is given by:

$$y_k = \left(\mathrm{h}_{d,k} + \mathrm{h}_k \Phi \mathrm{H}_1\right) \mathrm{w} s + n,$$

where s is the transmitted symbol with $\mathbb{E}[|s|^2] = 1$ and n is an additive white Gaussian noise term with variance σ^2.

Hence, the SNR in position k is given by

$$\mathbf{SNR}_k = \frac{\left|\left(\mathbf{h}_{d,k} + \mathbf{h}_k \boldsymbol{\Phi} \mathbf{H}_1\right)\mathbf{w}\right|^2}{\boldsymbol{\sigma}^2}.$$

Given a desired area where a single-antenna RX can be blocked in terms of line-of-sight signal coverage from the BS, RISs can influence 2.4 performance by realizing beams with reconfigurable widths. In fact, a variable-width AroI can ensure service delivery in an intended geographical area, while minimizing the need for the RIS reconfiguration, which requires computational cost for its optimization as well as RIS reflection sweeping power. According to the systematic approach of [JAS21] for the case where a RIS is placed in the LOS of a mobile UE (see Figure 3-8), a targeted AroI can be realised by mapping its points to the points in the surface of the RIS. In practice, the RIS gets partitioned into sub-surfaces which are intended to illuminate (i.e. enable acceptable QoS/coverage) the center of the sub-regions the entire desired/targeted area gets split into. To the purpose, it suffices to formulate a mapping from each RIS area point to each point in the targeted AroI. Based on such a mapping, the corresponding RIS phase shift for a wide AroI can be expressed by:

$$\boldsymbol{\mathcal{U}} = \{\boldsymbol{k} : \mathbf{SNR}_{\boldsymbol{k}} \geq \boldsymbol{t}\}.$$

The considered simulation scenario is the one described in sub-section 3.1.1 with the channel parameters in Table 3-1. Furthermore, we set $t = 100$ dB. We optimise the RIS phase shifts and BS precoding for the nominal RX position as described in sub-section 3.1.1.

Next, we evaluate the SNR received by a receiver located in any other position identified by the regular lattice for the optimised RIS and BS configuration of the previous subsection.

To investigate the spatial localization of the reliability performance, we use a binary contour plot in 2D, which is provided in the following. In particular, we show the 2D area where the two following conditions are met simultaneously: (i) given SNR threshold is reached thanks to the use of RIS, (ii) a standard system utilizing only precoding at the BS does not attain such minimum acceptable value.

In Figure 3-4, we analyze the case where there is no attenuation between the BS and the nominal RX position. Thanks to the passive beamforming at the RIS, the 2D area in which the received SNR is above the threshold t is enlarged in both the area around the direct link between the BS and the RIS and in the direction of the nominal RX position w.r.t the RIS.

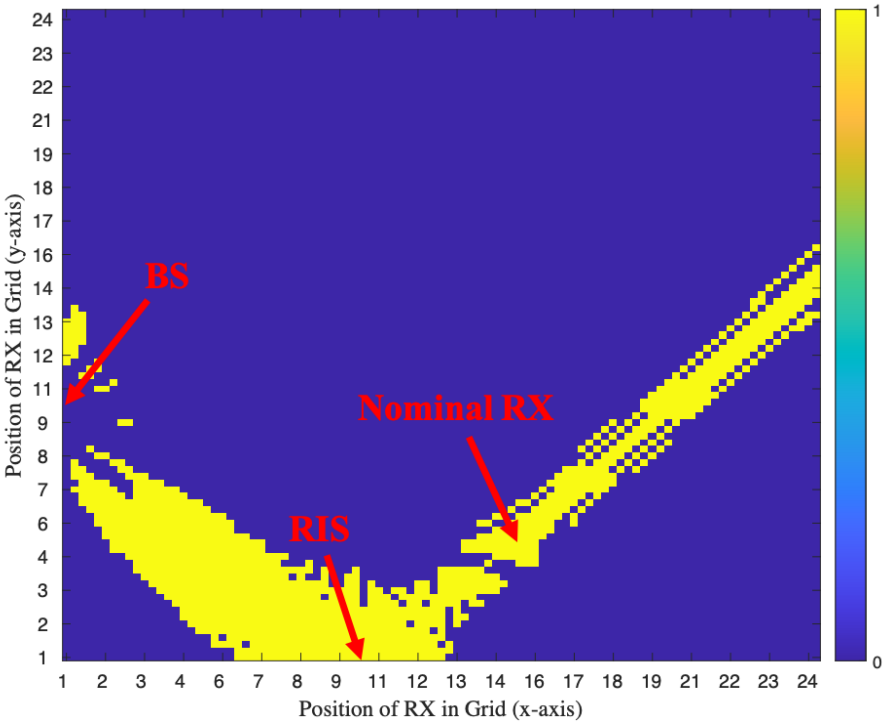

Figure 3-4 – DL case only: example of achievable reliability values in the absence of attenuators, where thanks to the RIS the received SINR is sufficient for successful decoding of the incoming signal whereas it is not with the standard technology.

Lastly, Figure 3-5 shows the spatial localization of the reliability metric in the case when there is an attenuator in the LoS link between the BS and the nominal RX position. We observe that due to the presence of the attenuator the substantial improvement is limited to the close proximity to the RIS and along the direction of the nominal RX position w.r.t the RIS, i.e., along the direction of beamforming at the RIS.

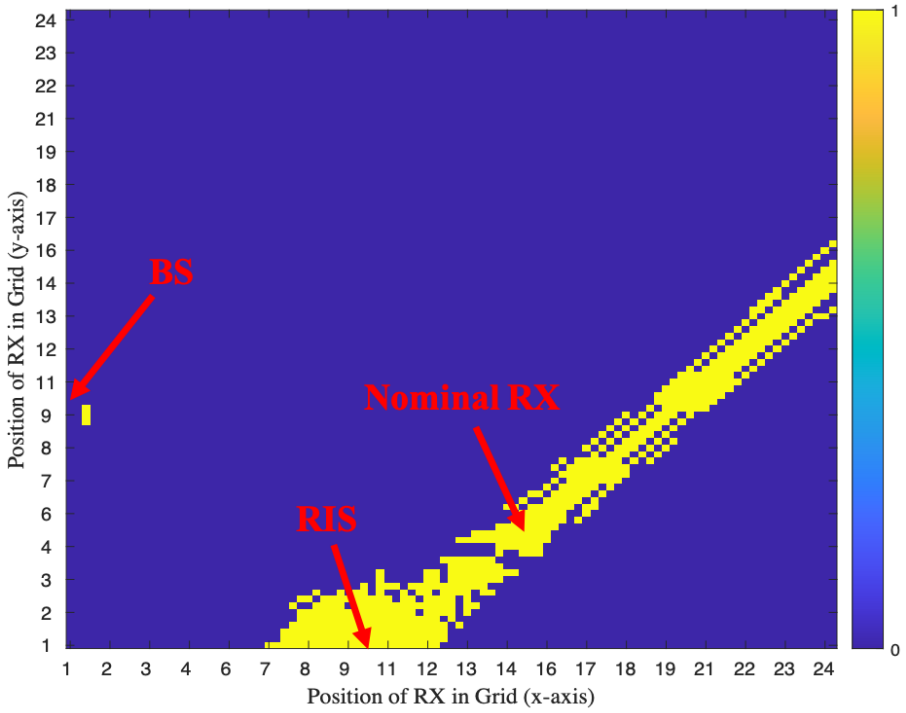

Figure 3-5 – DL case only: example achievable reliability values in the presence of an attenuator, where thanks to the RIS the received SINR is sufficient for successful decoding of the incoming signal whereas it is not with the standard technology.

3.1.2.2 Spatial focusing of latency

In this sub-section, we evaluate the effect of RIS in boosting latency for a nominal RX position. Thus, given the SNR definition given in sub-section 2.1 the communication latency (expressed in seconds) at position k, needed to transmit A_k bits over a channel with bandwidth B, is given by

$$L_k = \frac{A_k}{B\, log_2\left(1 + \frac{\left|\left(\mathbf{h}_{d,k} + \mathbf{h}_k \Phi \mathbf{H}_1\right)\mathbf{w}\right|^2}{\sigma^2}\right)}.$$

Assuming the case of a single RX and using the aforementioned definition of communication latency[3], we redefine the set of positions where L_k is guaranteed to be below a given threshold:

$$\mathcal{U} = \{k : L_k \leq l\}.$$

The considered simulation scenario is the same used in the previous sub-section, obtained optimising the RIS phase shifts and BS precoding for the nominal RX position as described in sub-section 3.1.1. Then, we evaluate the latency perceived by a receiver located in any other position identified by the regular lattice for the given RIS and BS configuration. The parameters used for the simulation are $A_k = 1$ Mbit and $B = 30$ MHz. The latency constraint is set to $l = 1$ ms.

To assess the spatial localization of the latency boost given by the RIS, a 2D representation visualizing and quantifying the regions of space where the optimized RIS for the single nominal RX position provides a substantial improvement. In particular, using a 2D binary contour plot, we illustrate the regions where the two following conditions are met simultaneously: (i) the given

[3] It is important to emphasize that, based on the definition given in section 2.3, latency involves also uplink transmission, i.e. latency is not just proportional to the higher downlink rate.

latency constraint is met thanks to the use of the RIS, (ii) a standard system would fail in obtaining the desired performance.

In Figure 3-6, we illustrate the acceptable latency values in a scenario where there is no attenuation between the BS and the nominal RX position. As we can see from Figure 3-6, the 2D latency boosted area is enlarged in both the area around the direct link between the BS and the RIS and in the direction of the nominal RX position w.r.t the RIS.

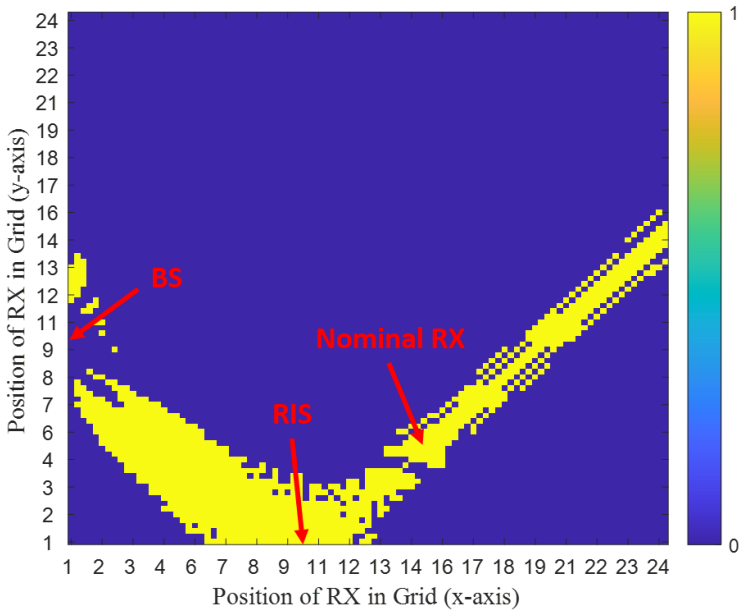

Figure 3-6 – Example of acceptable latency values in the absence of attenuators, where thanks to the RIS the perceived latency meets the desired performance constraint.

Finally, Figure 3-7 shows the acceptable latency values in the case when there is an attenuator in the LoS link between the BS and the nominal RX position. From Figure 3-7, we notice that, similarly to what happens for the reliability case of the previous subsection, the improvement of latency is limited to the close proximity to the RIS and along the direction of beamforming at the RIS.

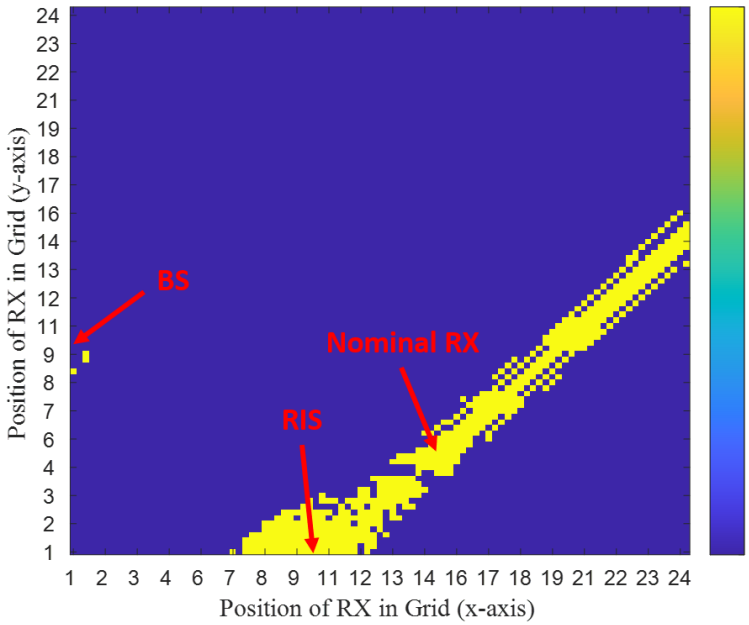

Figure 3-7 – Example of acceptable latency values in the presence of attenuators, where thanks to the RIS the perceived latency meets the desired performance constraint.

3.2 Characterisation of the area of influence

The following sub-section 3.2.1 presents a viable approach for RISs to influence the communication link performances by realizing beams with reconfigurable width.

The next sub-sections in this section are intended to describe the concept of AroI applied to different kinds of “boosted” areas corresponding to different parameters of interest influenced by RISs.

3.2.1 Area of Influence with variable beamwidth of the reflected beam

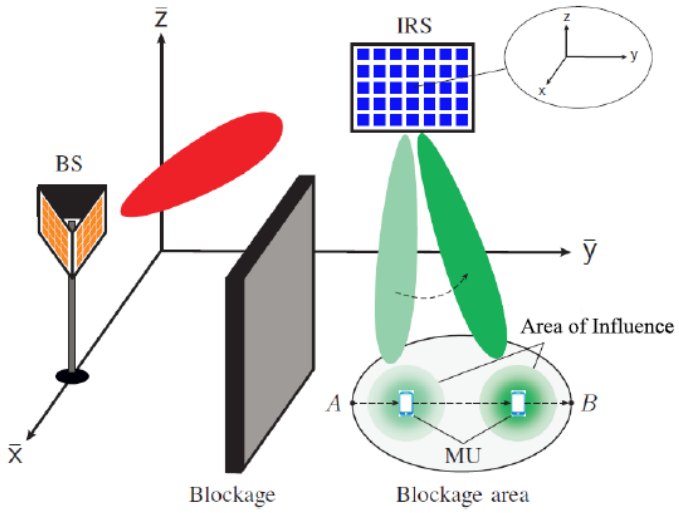

Figure 3-8 Considered RIS-assisted downlink communication system of [JAS21]. The RIS realises reflection beams of adjustable widths in order to provide acceptable link performance in a given geographical area.

Given a desired area where a single-antenna RX can be blocked in terms of line-of-sight signal coverage from the BS, RISs can influence the communication link's performance by realising beams with reconfigurable widths. In fact, a variable-width AroI can ensure service delivery in an intended geographical area, while minimising the need for the RIS reconfiguration, which requires computational cost for its optimization, as well as RIS reflection sweeping power. According to the systematic approach of [JAS21] for the case where a RIS is placed in the LOS of a mobile UE (see Figure 3-8), a targeted AroI can be realised by mapping its points to the points in the surface of the RIS. In practice, the RIS gets partitioned into sub-surfaces which are intended to illuminate (i.e., enable acceptable QoS/coverage) the center of the sub-regions the entire desired/targeted area gets split into[4]. To that purpose, it suffices to formulate a mapping $M(\boldsymbol{p})$ from each RIS area point $\boldsymbol{p}$, to each point $\mathbf{p}_r$ in the targeted AroI. Based on such a mapping, the corresponding RIS phase shift for a wide AroI can be expressed by:

$$\boldsymbol{\omega_W}(\boldsymbol{p}, \boldsymbol{P_{AroI}}) = \boldsymbol{\omega_F}\big(\boldsymbol{p}, \boldsymbol{M}(\boldsymbol{p})\big) - \boldsymbol{\kappa}\|\boldsymbol{M}(\boldsymbol{p}) - \boldsymbol{p_{RIS}}\|,$$

where P_{AroI} and $\boldsymbol{p}_{RIS}$ denote the set of points in the desired AroI and the RIS center coordinates, respectively. In addition, $\kappa = {}^{2\pi}/_{\lambda}$ is the wave number and $\omega_F\big(\boldsymbol{p}, M(\boldsymbol{p})\big) = -\kappa\|M(\boldsymbol{p}) - \boldsymbol{p}\| - \varphi(\boldsymbol{p})$, where $\varphi(\boldsymbol{p})$ denotes the impinging signal's phase. In the above expression, the term $\|M(\boldsymbol{p}) - \boldsymbol{p}_{RIS}\|$ is the reference distance from each point $M(\boldsymbol{p})$ to the RIS distance center, such that $\kappa\|M(\boldsymbol{p}) - \boldsymbol{p}_{RIS}\|$ only contributes at the focus point and not to the corresponding power.

Next, letting $M(\boldsymbol{p}) = \left[\frac{\Delta}{L}z + x_i, \frac{\Delta}{L}y + y_i, z_i\right]$, which corresponds to a square blockage area $\Delta \times \Delta$ for the targeted AroI, leads to

$$\boldsymbol{\omega_W}(\boldsymbol{p}, \boldsymbol{P_{AroI}}) = -\boldsymbol{\kappa}(\|\boldsymbol{M}(\boldsymbol{p}) - \boldsymbol{p}\| - \|\boldsymbol{M}(\boldsymbol{p}) - \boldsymbol{p_{RIS}}\|) - \boldsymbol{\varphi}(\boldsymbol{p}),$$

which means, in practice, that each part of the RIS locally focuses on one point in the set P_{AroI}, and the phase shift across the RIS gradually varies in such a way that all points in P_{AroI} are influenced. As depicted in Figure 3-9, the areas that meet the SNR requirement of $\gamma_{thr} = 10$ dB along (x, y)-axis are (20,10) m and (3,1.2) m corresponding to the carrier frequencies 3 GHz and 28 GHz using $\Delta = 8$ m and $\Delta = 1.5$ m, respectively.

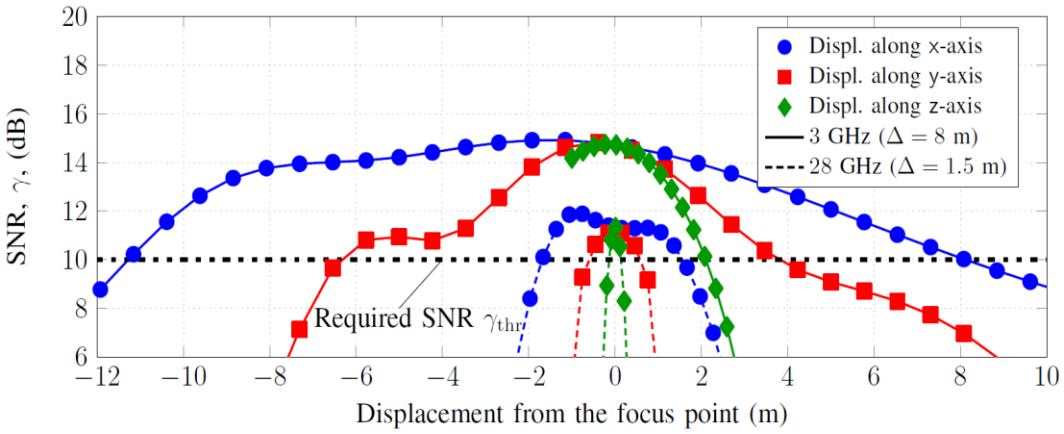

Figure 3-9 Received SNR vs. displacement along the x- y- and z-axes around the focused MU position.

[4] It must be noted that RIS phase optimisation is typically based on the explicit or implicit knowledge of the involved communication channel. So, while the communication channel changes, the RIS needs to be re-optimised, which entails the introduction of a large overhead (for control, channel knowledge, and optimisation). According to the current approach, data communication over the link starts with the area to be illuminated, instead of a specific position in it (re-configuration overhead gets reduced), and only when the desired QoS is not met, another beam that fits the area (or position of the user) to be served gets used.

3.2.2 EE-boosted area of influence

We recall that the EE of a DL communication between the network and a target or *intended* UE is the ratio of the spectral efficiency delivered to the target UE divided by the total power consumed in the radio network to that purpose.

The ***EE boosted area of influence*** (EE-AroI) is a representation visualising and quantifying in which *locations of the target UE*, RIS could improve significantly *the nominal EE of a standard system/technology*. In other terms, out of the EE-AroI, there is no way for the RIS to improve significantly EE.

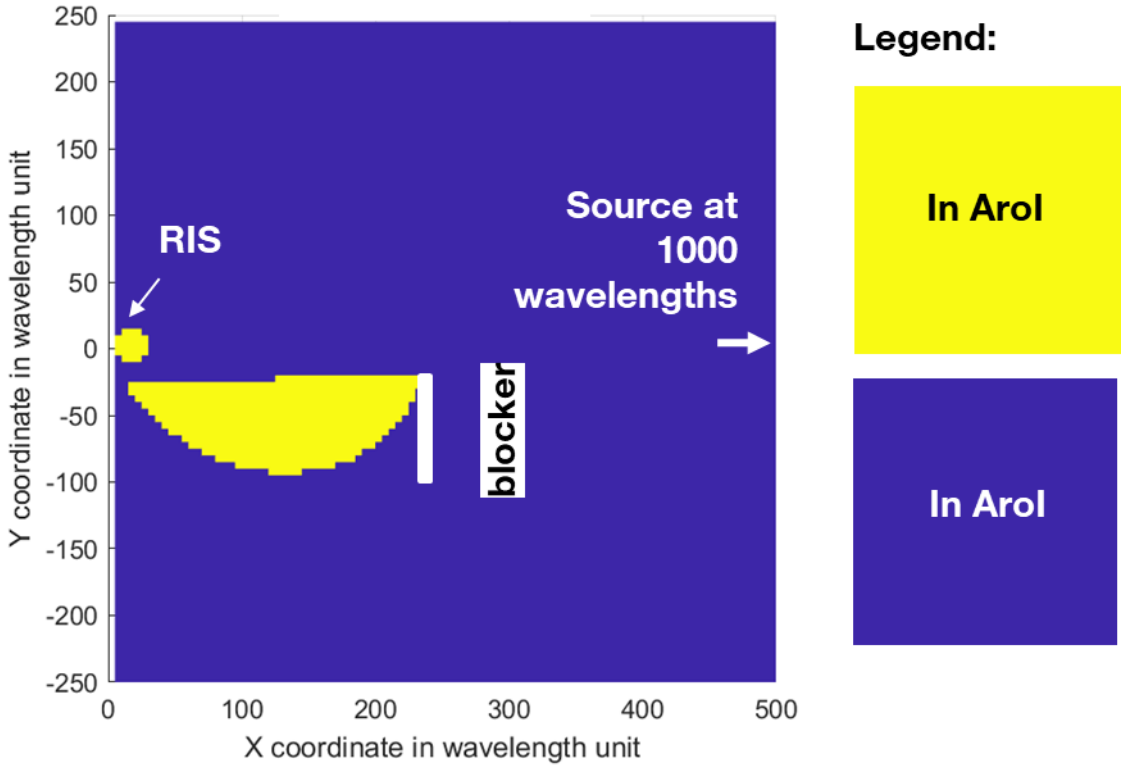

Figure 3-10 – Example of EE-boosted area, where the received power at the target user has been boosted by at least 3 dB.

It can be typically represented as a binary contour plot in 2D as illustrated in Figure 3-10 au-dessus with a RIS consisting of a uniform linear array of 16 unit-cells (10 dBi directional patch antennas) spaced by half a wavelength and with ideal phase-shift control. In the AroI, *the target user* can experience a received power that is *at least boosted by 3 dB* when the RIS is present compared to when the RIS is absent. The computed received power with RIS, is an upper bound, obtained with RIS weights making sure that all the paths (direct source-target user, reflected paths) combine coherently at the target user. Note that in Figure 3-10, the AroI is composed of two separate areas: a tiny one, close to the RIS and in visibility of the source, and a larger one, in the visibility of the RIS and in non-line-of-sight of the source, due to a blocking wall. Hence, *the EE-AroI of a RIS depends on its propagation environments and especially on blockers*.

Figure 3-11 au-dessous illustrates the EE-boosted area in a more complex deployment and propagation scenario. In this case, as illustrated in Figure 3-11 a), we consider as a source a massive multiple input multiple output (M-MIMO) BS performing adaptive BF, using the so-

called maximum ratio transmission (MRT) BF, at 3.7 GHz. The M-MIMO BS covers a building. The whole propagation environment does exist in Belfort city, France, and has been captured in a 3 dimensional (3D) ray tracing tool internal to Orange taking into account propagation paths in 3D. Figure 3-11 b) illustrates the received power in one room of the building, when MRT BF is activated (for each position, the received power takes into account the BF gain) and **without RIS**. We can observe that all positions in LOS of the BS (through a window) get strong signal (positions colored in bright yellow). On the contrary, positions in the shade of the walls, experience much lower performance (positions colored in dark blue). As illustrated in Figure 3-11 a), we place a RIS against the wall that is in LOS of the BS to ensure it is well illuminated by the BS. This time, RIS weights are computed in such a way that the RIS is "electronically tilted" in the direction of the target user (in other terms, if all elements of the RIS were hit by a wave in boresight, then this wave would be reflected in the direction of the target user). Hence, for any position of the target user in the room, the BS performs MRT BF towards the target user, in a propagation environment where the RIS is already "pre-tilted" in the direction of this target user. Figure 3-11 c), illustrates the EE-AroI, i.e. the positions (in yellow) where the received power with RIS (and BF gain) exceeds the received power without RIS (and still with BF gain) by more than 3 dB. Thanks to the RIS, the areas in the shade of the walls can be boosted by at least 3dB. In such complex environment, the shape of the EE-AroI is much more complex and difficult to predict.

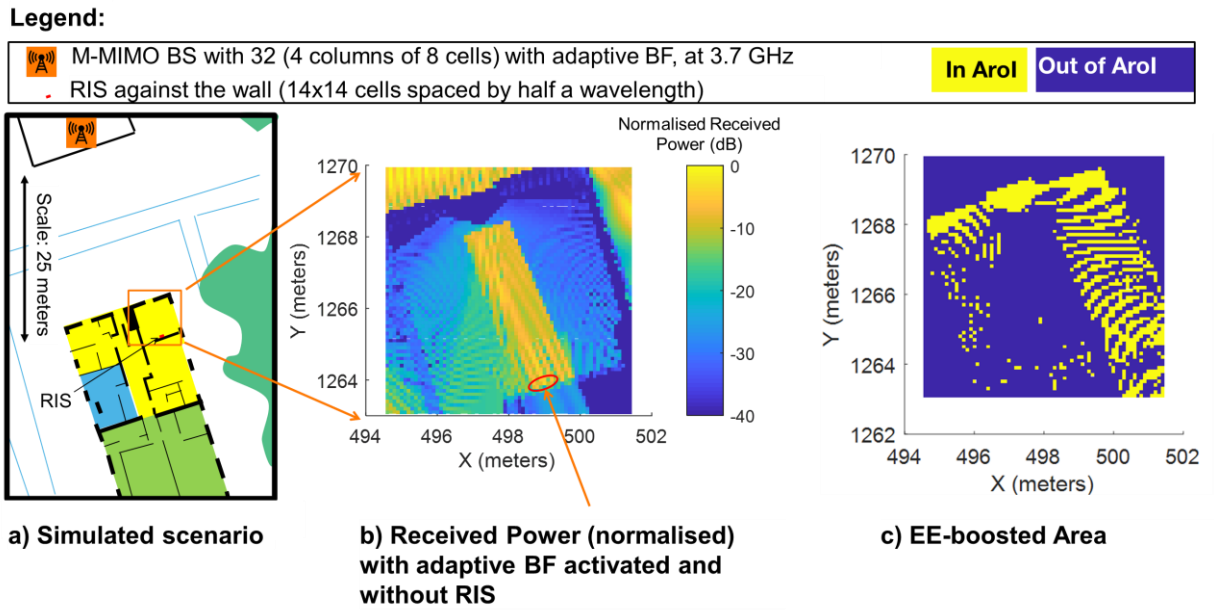

Figure 3-11 – Example of EE-boosted area, where the received power at the target user has been boosted by at least 3 dB, in a complex propagation environment.

3.2.3 SE-boosted area of influence

As a further study on the locality of a RIS and how it formulates the space around it, we examine the SE in a sub-grid of the considered grid in Section 3.1.1. Specifically, instead of using the solution given at a nominal position of the RX which results in SE spatial focusing, in this subsection we solve the optimisation problem for each position of the sub-grid and then plot the 2D contour figures as shown in Figure 3-12 and Figure 3-13. Figure 3-12 depicts the case when a RIS is not present in the considered system, for the case of a strong LoS component for the direct channel $\mathbf{h}_d$, as well as the case where the attenuation factor of Section 3.1.1 is considered. As shown, it is evident that when an attenuator is present, the SE for each grid position is smaller than the case without the attenuator.

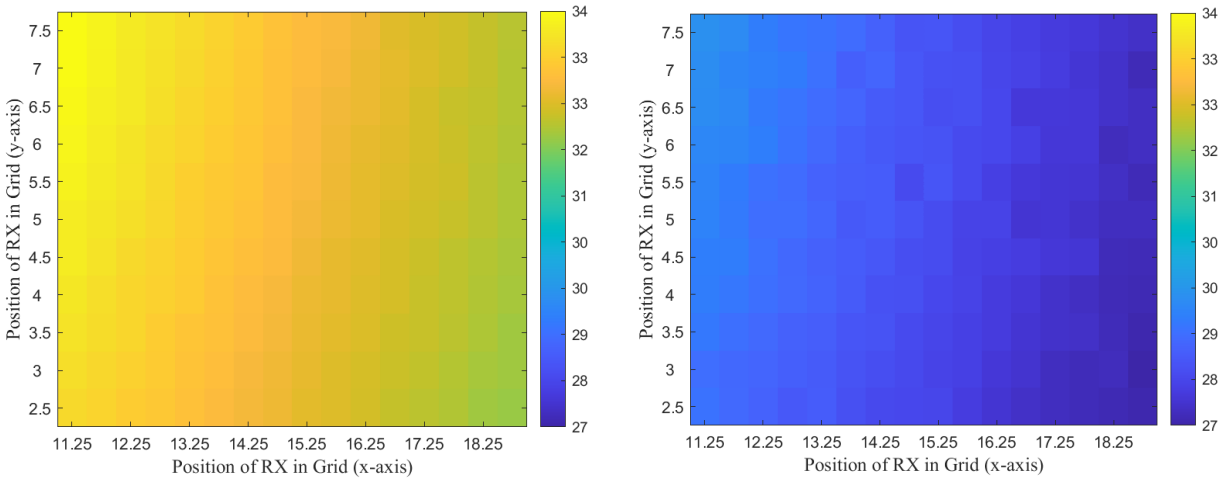

Figure 3-12 – SE on a 2D sub grid without a RIS. (Left) without attenuation factor for the direct link between BS and RX. (Right) with attenuation factor equal to 0.01.

On the other hand, when a RIS is present (Figure 3-13) the whole area is boosted in terms of the higher achievable rates' values that are observed. Moreover, both subfigures are very close to each other since the effect of the RIS is almost the same either in the case without attenuator or with. Finally, it is observed that the higher values in both heatmaps of Figure 2-11, are observed towards the location of the RIS, which is placed outside the depicted sub grid.

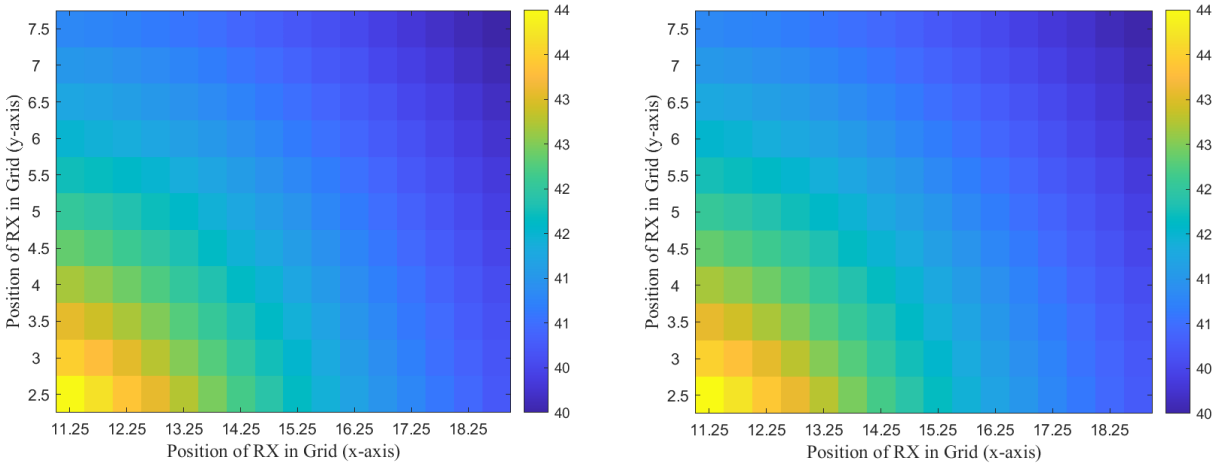

Figure 3-13 – SE on a 2D sub grid with the presence of a RIS. (Left) without attenuation factor for the direct link between BS and RX. (Right) With attenuation factor equal to 0.01.

3.2.4 SSE-boosted area of influence

As another example for the AroI of a RIS and SSE, we next consider a sub grid of the one in Figure 3-3 and solve the corresponding optimisation problem for each position of it, to examine the effect of a RIS. As it is shown, when a RIS is not present the SSE values are much smaller than the case where a RIS is present, which shows how a RIS boosts the area under consideration. Moreover, it is also observed that a line pattern is formulated in both cases, but in a different way (since their slopes are different). In the case without a RIS, the formulated line pattern matches with the direction of the line which connects the BS and the intended RX, since the RX is placed at the centre of the sub grid. Therefore, when the eavesdropper lies along this line, smaller secrecy rate values are observed. Similarly, when a RIS is placed on the wide grid,

the line with smaller secrecy rate values lies on the direction that connects the RIS with the RX and accordingly when E is located at those positions.

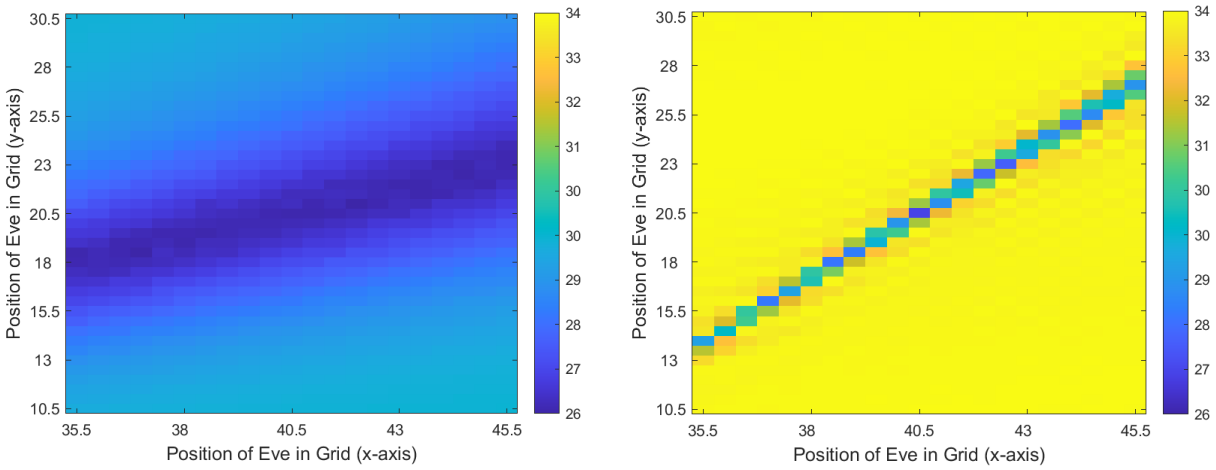

Figure 3-14 - SSE Secrecy Spectral Efficiency on a 2D sub grid without a RIS (Left). With a RIS (Right).

3.2.5 EMFEU-boosted area of influence

We recall that the EMFEU of a DL communication between the network and a target UE is the ratio of the spectral efficiency delivered to the target UE, divided by the EMFE of an exposed non-intended user (see sub-section 2.10).

The **EMFEU-boosted area of influence** (EMFEU-AroI) is a 2D representation visualising and quantifying in which locations of the exposed non-intended user the RIS would reduce the nominal exposure of a standard system/technology. In other terms, out of the EMFEU-AroI there is no way for the RIS to significantly reduce the exposure.

It can be typically represented as a binary contour plot in 2D as illustrated in Figure 3-15 with a RIS consisting of a uniform linear array of 16 unit-cells (10 dBi directional patch antennas) spaced by half of the wavelength. In the AroI, the *non-intended user* can experience a received power that is *at least reduced by 3 dB* when the RIS is present compared to when the RIS is absent. The computed received power with RIS, is an upper bound, obtained with RIS weights making sure that all the reflected paths combine coherently together, at the non-intended UE, but *in opposition* to the direct source-to-user path. Figure 3-10, the AroI is, composed of two separate areas: a tiny one, close to the RIS and in visibility of the source, and a larger one, in the visibility of the RIS and in non-line of slight of source, due to a blocking wall. Hence, *the EMFEU-AroI of a RIS depends on its propagation environments, and especially on blockers***.**

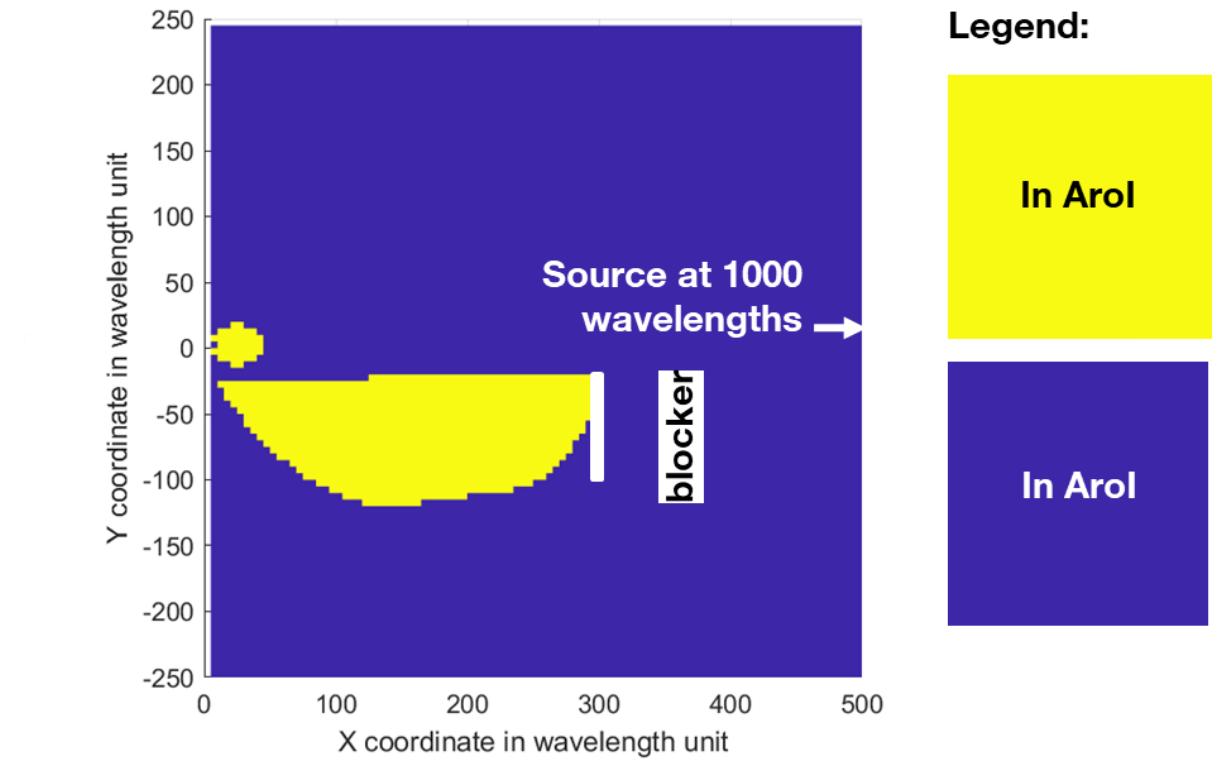

Figure 3-15 – DL case only, Example of EMFEU-AroI where the received power at the exposed non-intended UE has been reduced by at least 3 dB

3.2.6 Localisation-enabled area of Influence

The ***localisation-enabled area of influence*** (LE-AroI) is a 2D representation intended to visualise and quantify where RIS can restore *service coverage & continuity*, when conventional localisation is not feasible or strongly degraded, typically if:

- The number of active BS(s) is by default insufficient to ensure non-ambiguous localisation;
- The number of BS(s) is sufficient, but the system is facing local blockage situations over one or several radio links.

It can be typically represented as a binary contour plot in 2D, accounting for the area where localization is theoretically feasible (e.g., where PEB is defined) and/or where the achievable error is below a certain a-priori threshold (i.e., where 2D-RMSE or PEB < Target).

A. *Example of PEB with 1 single BS and 1 RIS in reflection mode*

In Figure 3-16 and Figure 3-17, we show two examples of PEB contour map characterising the localisation error over a 2D scene for a RIS-enabled single-BS single input single output (SISO) system, with random and directional RIS phase profiles respectively.

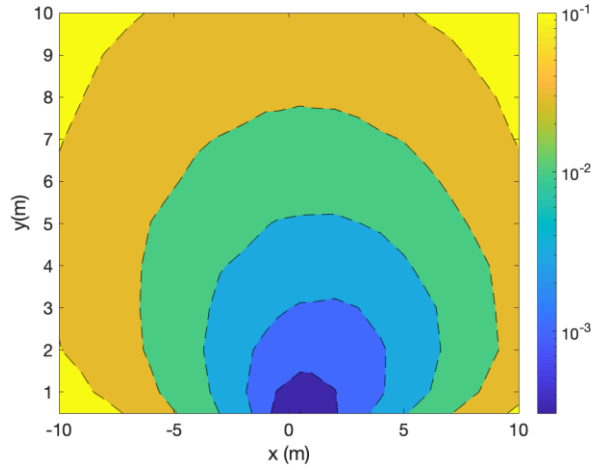

Figure 3-16 – Example of PEB for a RIS-enabled SISO system with random RIS configuration, RIS at the origin, UE on the plane [x, y, -y], and BS at [5, 5, 0].

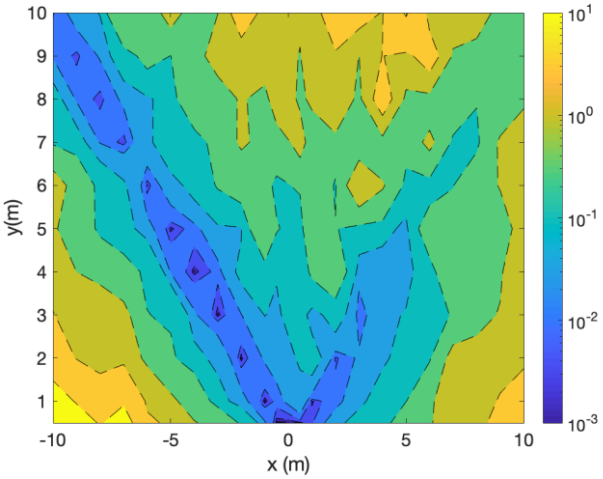

Figure 3-17 – Example of PEB for a RIS-enabled SISO system with directional RIS configuration directed at [-1, 1, -1].

B. Example of PEB with multiple RISs in receive mode

In Figure 3-18 (a)-(c), according to an indoor localisation with multiple RISs in reception mode, the PEB in dB is shown for a UE positioned on the z=5m plane. Free space pathloss is considered and LoS channels. 3 RISs are deployed, equipped with single RX RF chains, with 64 elements each, located for case (a) at [0, 5, 7], [5, 0, 1] and [10, 6, 8], for case (b) at [0, 1, 7], [1, 0, 1], [5, 0, 8], and for case (c) at [0, 9, 2], [1, 10, 8] [3, 10, 4]. We observe that for (a) there is an area located between the RISs where the PEB takes lower values than the rest of the grid. Comparing case (a) with cases (b) and (c), it is obvious that by locating the RISs towards one corner of the room, the area showing lower PEB, moves to that specific corner. Moreover, by placing the RISs closer to each other in case (c) than in case (b), the low-PEB area becomes more pronounced. We conclude that the location of the RISs plays an important role for the performance of localisation and by optimising their placement one could optimise the localisation in certain areas.

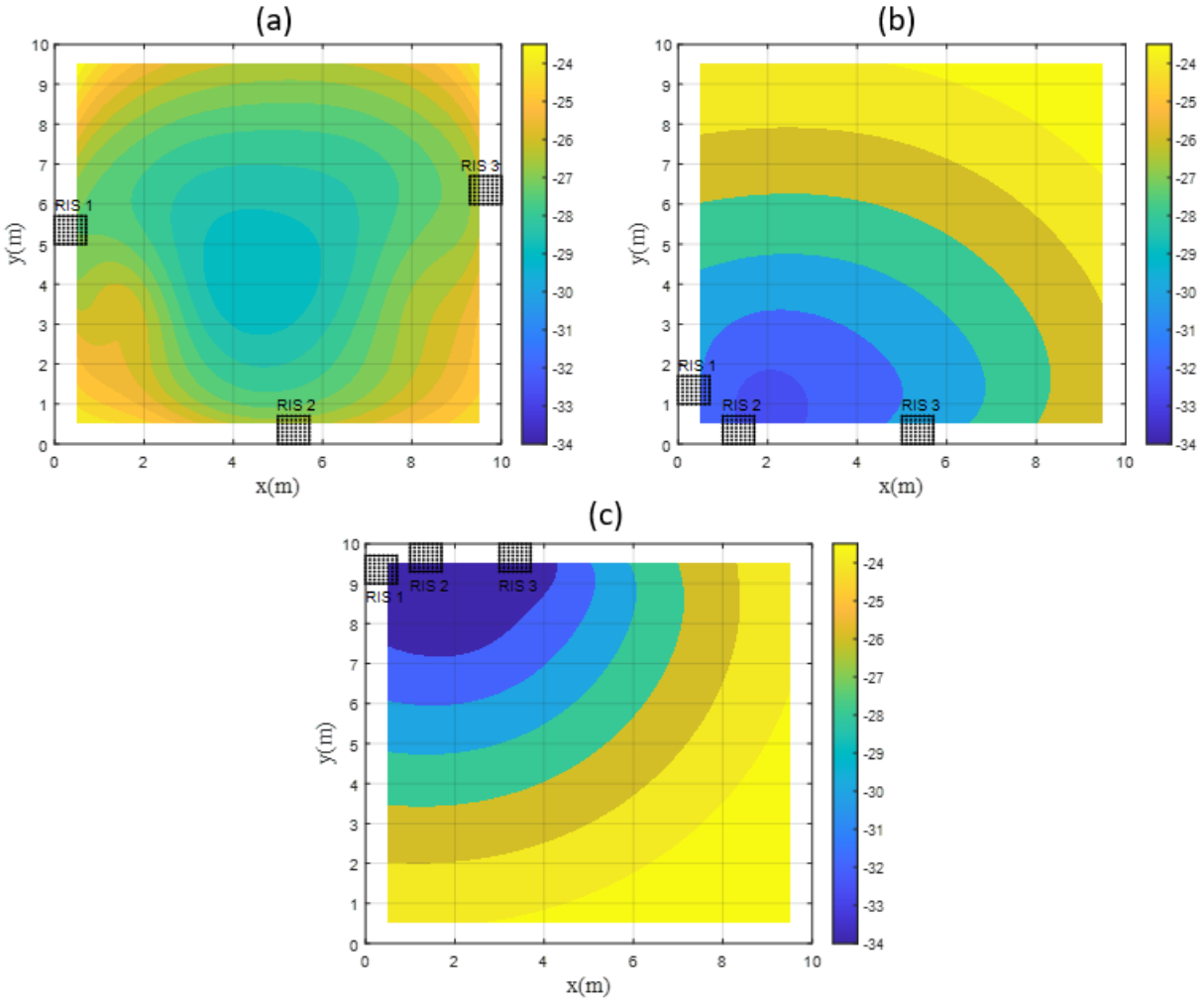

Figure 3-18 – Examples of PEB (in dB) for an indoor localisation system with 3 RISs in receive mode located for (a) at [0, 5, 7], [5, 0, 1], [10, 6, 8], for (b) at [0,1,7], [1,0,1], [5,0,8], and for (c) at [0, 9, 2], [1, 10, 8] [3, 10, 4].

3.2.7 Localisation-boosted area of influence

The **localisation-boosted area of influence** (LB-AroI) is another 2D representation visualising and quantifying where RIS would improve the *nominal accuracy of a standard system/technology*, which is already operating in favourable conditions (e.g., showing that, given an a priori BS deployment, RIS can timely/locally improve the accuracy to fulfil specific UEs'/application requirements). The LB-AroI can thus be simply defined as the area where the achievable error with RISs is lower than that with no RIS. Just like the LE-AroI, it can be typically represented as a binary contour plot in 2D.

We detail hereafter the example of PEB with multiple BS(s) and multiple RISs in reflection mode. In Figure 3-19 (a)-(d), we show additional examples of PEB contour plots illustrating both RIS-boosted localisation performances and RIS-aided low-profile localization in a SISO system through the use of RISs in reflection mode. In these examples, we assume a transmit power of 0.1 mW (-10 dBm) at active BS(s), 3 successive DL transmissions over 1500 subcarriers with a frequency spacing of 240 kHz (thus, with a bandwidth of 360 MHz) per estimate per BS, a RIS size of 128 elements (set as a linear array), free-space propagation in all 2D locations systematically, as well as the possibility to exploit the near-field regime for location estimation.

First, in Figure 3-19 (a), we show the PEB of a reference system (i.e., non-RIS baseline) with 3 BS(s) located in [1, 19], [17, 17], and [8, 1]. On Figure 3-19 (b), we show the PEB while using one additional RIS in [10.0], when the RIS-reflected path is used all over the scene. In this case, we show that the gain is thus mostly noticeable when the UE is close enough from the 3rd transmitting BS, while it is more marginal in the rest of the scene (where direct path contributions are by far dominating). In Figure 3-19 (c), we show the PEB while assuming the presence of a 2nd RIS in [12, 0], while removing one of the 3 BS(s). In this case, we show that, in comparison with the conventional system based on 3 active BS(s), even if the performance is obviously globally degraded over a large portion of the 2D scene, the performance is still maintained at a fairly good level in a significant spatial sub-area close to the 2 RISs (i.e. offering a performance level comparable to that achieved in the inner part of the scene, when using the 3 active BS(s) in Figure 3-19 (a)), thus demonstrating lower-profile localisation capabilities (i.e., strictly adapted to local needs). Finally, while using the direct paths from the 3 available BS(s) systematically, but while making deliberately selective/parsimonious usage of an additional RIS-reflected path in a small sub-area (represented as a black rectangular area in the shown example), we illustrate the possibility to create arbitrary localisation-boosted sub-areas, which can be particularly relevant for multi-accuracy service provision (e.g., for Industry 4.0 applications).

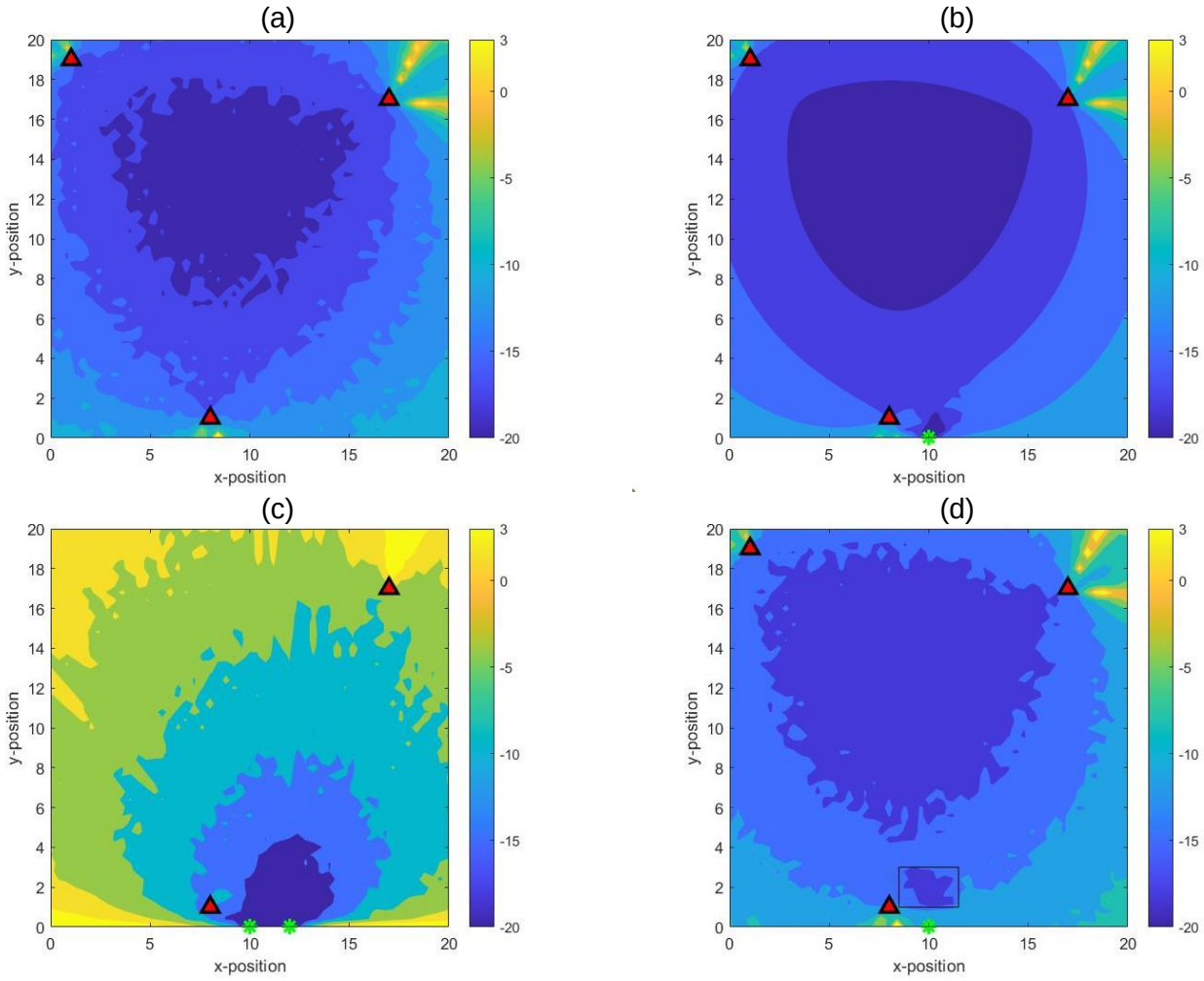

Figure 3-19 – Example of PEB (in dB) for (a) a conventional localisation system with 3 BS(s) in [1, 19], [17, 17], and [8, 1], (b) a RIS-boosted localisation system with the 3 previous BS(s) and one single RIS in [10, 0], (c) a RIS-aided low-profile localisation system with 2 active BS(s) only and a second RIS in [12, 0] and, finally, (d) the creation of an arbitrary localisation-boosted sub-

area assuming the selective use of the 1st RIS in addition to BS(s) in the black rectangular area only (and of the 3 BS(s) only over the rest of the scene).

4 RIS Band of Influence (BoI)

In this section, we investigate the spectrum co-existence between operators. Let us consider two operators “O1” and “O2” using distinct licensed spectrum bands as illustrated in Figure 4-1. “O1” is connected to a UE, and “O2” is operating a RIS.

Let us define as the bandwidth of influence (BoI), the frequency bandwidth in which, any wave hitting the RIS, will be reflected. As illustrated in Figure 4-1, we consider the case where the BoI of the RIS operated by “O2” has an overlap with the spectrum licensed to “O1”. As a consequence, when the waves generated by “O1” hits the RIS operated by “O2” they generated unwanted reflections towards the UE.

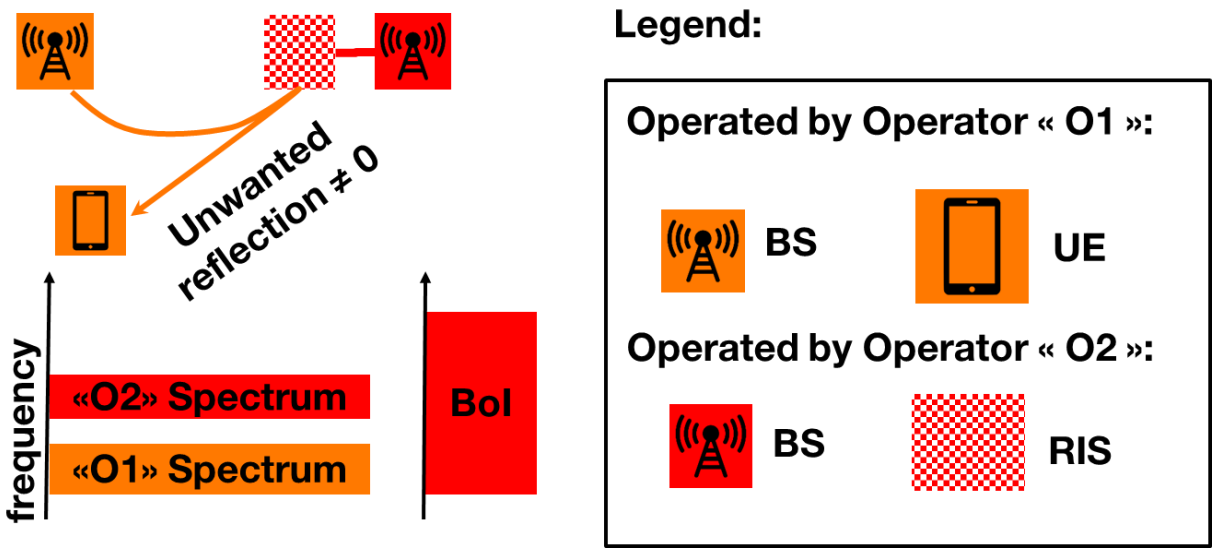

Figure 4-1 Unwanted reflections due to overlap between “O1” licensed spectrum and the BoI of the RIS operated by “O2”.

To better quantify the BoI, let us consider an existing ReflectArray antenna without its feeder (it has been shown in [FPH+21-1] and [FPH-21-2] that a ReflectArray antenna can be turned into a RIS by only withdrawing the antenna feeder). In this case, the cells of the antenna will reflect the incident wave coming from an external source instead of reflecting the incident wave generated by a close (in the near-field) source.

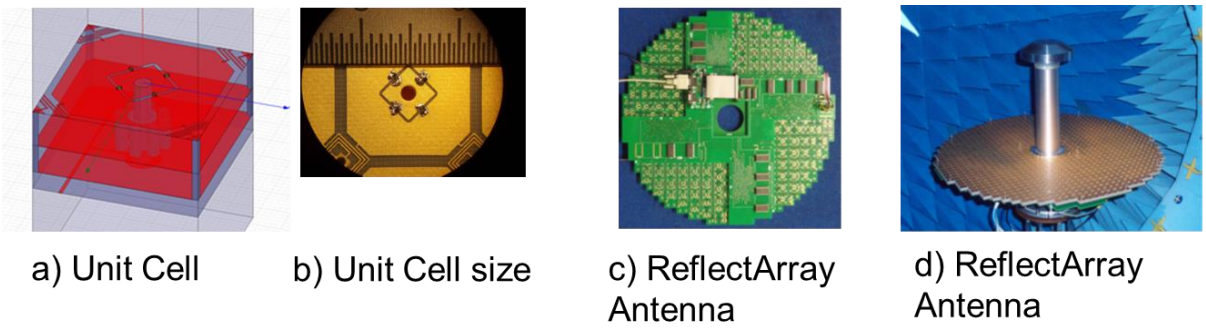

Figure 4-2 – Examples of ReflectArray Antennas.

Let us now consider an existing ReflectArray antenna detailed in [RBF+13] and illustrated in Figure 4-2. When one cell is illuminated by an incident wave, it backscatters it with a phase-shift that is controlled through varactors. The phase-shift of each cell is controlled individually. By

applying pre-computed phase-shift laws, one can obtain desired beams. Such ReflectArray antenna is designed to perform beamforming at 5.25 GHz, as illustrated by simulations in Figure 4-3.

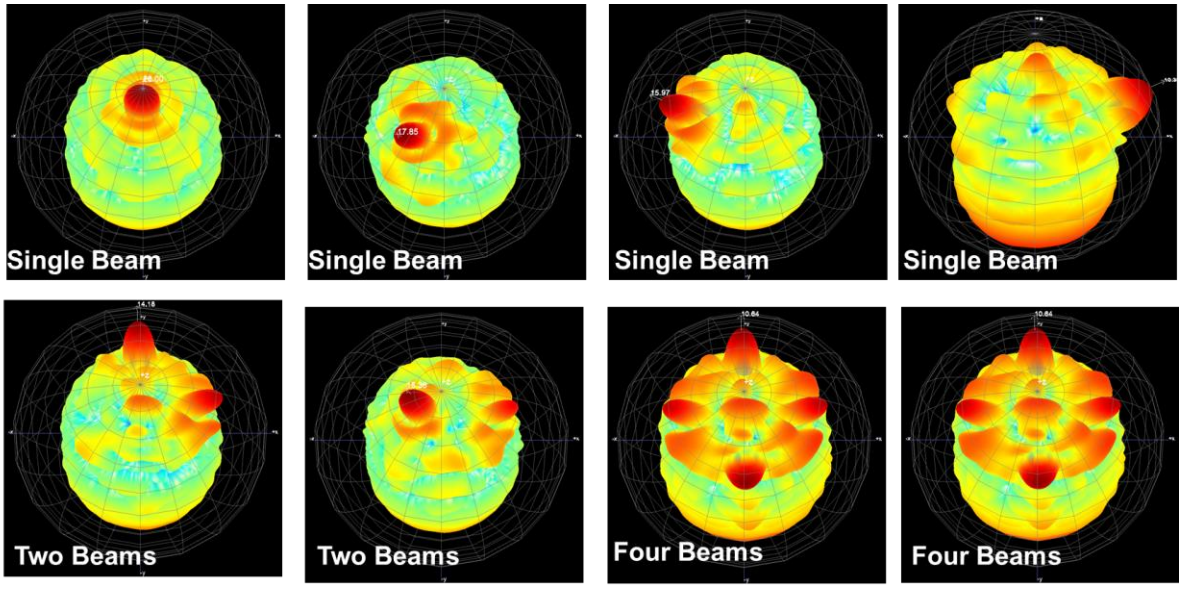

Figure 4-3 – Examples of beams obtained with the considered ReflectArray antenna.

However, such ReflectArray antenna has a large BoI. Figure 4-4 au-dessous, illustrates experimental measurements of the directivity and the gain of the ReflectArray antenna as a function of the carrier frequency of the incident wave, for four different configurations of the cells. More precisely, first, for a given configuration, the voltages of the varactors are set in order to obtain a target beam direction, at the operating carrier frequency of 5.25 GHz. Then, the ReflectArray is illuminated with waves at carrier frequencies different from the 5.25 GHz operating frequency. Carrier frequencies between 4.5 and 6 GHz are used. The following phenomena are observed:

- **Large BoI**: the ReflectArray reflects incident waves from 4.9 GHz at least to 5.9 GHz or even 6 GHz, in some configurations, therefore BoI can be as large as 1 GHz;
- **Variable BoI**: BoI is different for each configuration.

The second phenomenon is due to the fact that a cell being illuminated by an incident wave with a carrier frequency that is different from the operating carrier frequency, will backscatter the wave with a different phase shift, amplitude, and diagram.

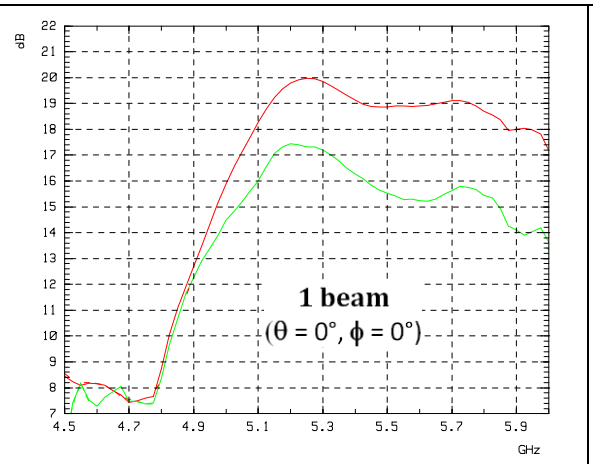

a) Configuration 1

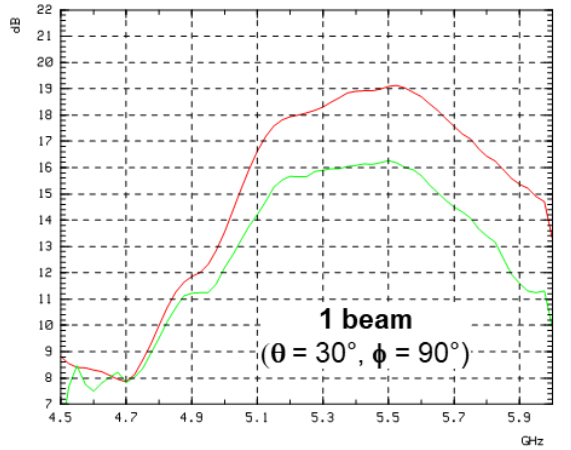

b) Configuration 2

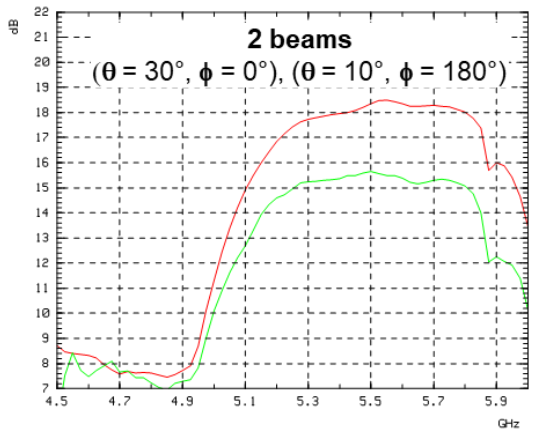

c) Configuration 3

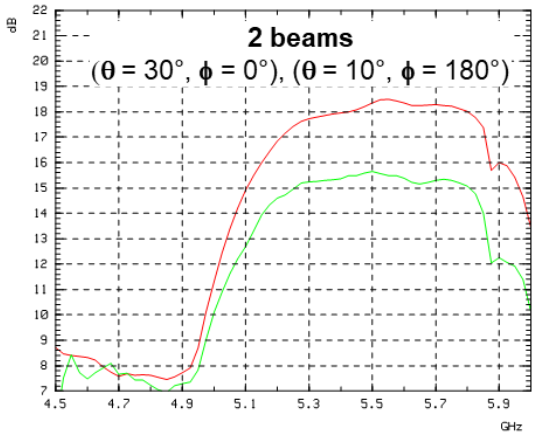

d) Configuration 4

Figure 4-4 – Directivity (red curve) and Gain (green curve) in dB as a function of the carrier frequency (between 4.5 and 6 GHz).

As a conclusion, the BoI of a real RIS deviates (maybe even significantly) from the behaviour of an ideal RIS which is expected to perfectly match the spectrum bandwidth of the operator it is operated by. Hence the impact of the introduction of a RIS on spectrum coexistence between operators must be studied and a characterisation/modelling of the BoI of a RIS needs to be necessarily derived.

5 Conclusions

All WP2 objectives have led relevant activities to identify classical and beyond-SoTA relevant performance metrics to be used by the technical WPs to assess the performance of RISE wireless systems for different scenarios. Among such metrics, target KPIs will be further discussed according to planned field-trials activities.

A generic DL system model has been described as the basis to provide the definitions for various performance metrics (the corresponding UL system model can be derived in a similar manner) to be used for evaluating the performance benefits brought by the RIS technology: signal to noise (plus interference) ratio, latency, communication reliability, channel estimation accuracy, localisation accuracy and integrity, energy efficiency, electromagnetic field exposure utility, secrecy spectral efficiency.

The concept of “Area of Influence” as the area of significant improvement of wireless connectivity enabled by the RIS technology has been introduced and some analysis has been performed. Current simulation results show that the improvement brought by the RIS optimisation, with respect to each of the considered connectivity metrics, is localised in space. Furthermore, in a common setup made of a single TX, a single RIS, a single intended RX and potentially an attenuator/blocker, after having optimised the system parameters for the position of the nominal intended RX, the substantial improvement of the performance, which lies on the path of the RIS-RX link (as well as the TX-RIS link, in case there is no attenuator), has been visually demonstrated for all metrics in a Ricean-faded channel with a strong LoS component.

Furthermore, the concept of “Band of Influence” has been introduced. Specifically, the definition is given by the bandwidth in which any wave hitting the RIS gets reflected. After an experimental investigation of its behaviour, it became evident the impact of the introduction of a RIS on spectrum coexistence between operators, which would require a characterisation/modelling of the BoI of a real RIS to face the significant deviations it shows with respect to ideal one.

6 References

[AKW+21] G. C. Alexandropoulos, K. Katsanos, M. Wen, and D. B. da Costa, "Safeguarding MIMO communications with reconfigurable metasurfaces and artificial noise," in Proc. *IEEE International Conference on Communications*, Montreal, Canada, 14–18 June 2021, pp. 1-6.

[CDP+20] A. Clemente, F. Diaby, Di Palma, L. Dussopt and R. Sauleau“Experimental validation of a 2-bit reconfigurable unit-cell for transmitarrays at Ka-band,” IEEE Access, vol.8, pp.114991-114997, 2020.

[CDS+12] A. Clemente, L. Dussopt, R. Sauleau, P. Potier and P. Pouliguen, "1-Bit Reconfigurable Unit Cell Based on PIN Diodes for Transmit-Array Applications in X -Band," in IEEE Transactions on Antennas and Propagation, vol. 60, no. 5, pp. 2260-2269, May 2012, doi: 10.1109/TAP.2012.2189716.

[CDS+13] A. Clemente, L. Dussopt, R. Sauleau, P. Potier and P. Pouliguen, "Wideband 400-Element Electronically Reconfigurable Transmit array in X Band," in IEEE Transactions on Antennas and Propagation, vol. 61, no. 10, pp. 5017-5027, Oct. 2013, doi: 10.1109/TAP.2013.2271493.

[DCS+20] F. Diaby, A. Clemente, R. Sauleau, K. Pham and L. Dussopt “2-bit reconfigurable unit-cell and electronically steerable transmit arrayat Ka-band,” IEEE Transaction Antennas and Propag., vol.68, no.6, pp.5003-5008, Jun.2020.

[DPC+17] L. Di Palma, A. Clemente, L. Dussopt, R. Sauleau, P. Potier and P.Pouliguen“Circularly-polarized reconfigurable transmit array in Ka-bandwith beam scanning and polarization switching capabilities,” IEEE Transaction on Antennas and Propag., Vol.65, no.2, pp.529-540, Feb.2017.

[HZA+19] C. Huang, A. Zappone, G. C. Alexandropoulos, M. Debbah and C. Yuen, "Reconfigurable Intelligent Surfaces for Energy Efficiency in Wireless Communication," in IEEE Transactions on Wireless Communications, vol. 18, no. 8, pp. 4157-4170, Aug. 2019, doi: 10.1109/TWC.2019.2922609.

[FPH+21-1] R. Fara, D.-T. Phan-Huy, P. Ratajczak, A. Ourir, M. Di Renzo, and J. de Rosny, “Reconfigurable Intelligent Surface -Assisted Ambient Backscatter Communications -- Experimental Assessment,” IEEE International Conference on Communications Workshop on Reconfigurable Intelligent Surfaces for Future Wireless Communications, 2021, Apr. 202. Available at: https://hal.archives-ouvertes.fr/hal-03358458.

[FPH+21-2] R. Fara, P. Ratajczak, D.-T. Phan-Huy, A. Ourir, M. Di Renzo, and J. De Rosny, “A Prototype of Reconfigurable Intelligent Surface with Continuous Control of the Reflection Phase,” Submitted to IEEE WCM, May 2021. Available at: https://arxiv.org/abs/2105.11862.

[JAS21] V. Jamali, G. C. Alexandropoulos, R. Schober, H. V. Poor, “Low-to-Zero-Overhead IRS Reconfiguration: Decoupling Illumination and Channel Estimation,” IEEE Commun. Lett., to appear 2022. Available at https://arxiv.org/pdf/2111.09421.pdf

[RBF+10] P. Ratajczak, J. M. Baracco and P. Brachat, "New measurement method of the reflection phase coefficient of High Impedance Surface," Proceedings of the Fourth European Conference on Antennas and Propagation, Barcelona, Spain, 2010, pp. 1-4.

[RBF+13] P. Ratajczak, P. Brachat, J. Fargeas and J. Baracco, "C-band active reflectarray based on high impedance surface," 2013 IEEE International Symposium on Phased Array Systems and Technology, Waltham, MA, USA, 2013, pp. 570-576, doi: 10.1109/ARRAY.2013.6731892.

[ZDR+21-1] A. Zappone, M. Di Renzo, F. Shams, X. Qian, M. Debbah “Overhead-Aware Design of Reconfigurable Intelligent Surfaces in Smart Radio Environments”. Available at https://arxiv.org/pdf/2003.02538.pdf

[ZDR+21-2] A. Zappone, M. Di Renzo, F. Shams, X. Xi, M. Debbah “On The Optimal Number of Reflecting Elements for Reconfigurable Intelligent Surfaces” available at https://arxiv.org/pdf/2007.07665.pdf